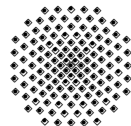


Phase Field Approaches to Topology Optimization

Yi Hu

Institute of Applied Mechanics (CE) · Chair I · Prof. C. Miehe
University of Stuttgart, 70569 Stuttgart, Pfaffenwaldring 7, Germany



Contents

- 1. Introduction.**
- 2. Basics of Topology Optimization.**
 - 2.1. Problem Formulation.
 - 2.2. SIMP.
 - 2.3. Level Set Method.
 - 2.4. Phase Field Method.
 - 2.5. Specific Issues.
- 3. Phase Field Approach.**
 - 3.1. Interface Representation.
 - 3.2. Phase Field Models.
 - 3.3. Takezawa's Approach.
 - 3.4. Wallin's Approach.
- 4. Numerical Formulation and Implementation.**
 - 4.1. Augmented Lagrangian Method.
 - 4.2. Evolution of Design Variable.
 - 4.3. Topology Optimization with Augmented Lagrangian Method.
 - 4.4. Overview of Implementation.
- 5. Numerical Results.**
 - 5.1. Cantilever Compliance Problem.
 - 5.2. Thermomechanical Problem.
 - 5.3. Coupled Electro-mechanical Unit Cell Optimization.
- 6. Conclusion.**
- A. Detailed Comparison of TK10 and WL13.**

Master Thesis supervised by Dipl.-Ing. Matthias Rambausek
and Jun.-Prof. Dr.-Ing. Marc-André Keip
Stuttgart, Sept. 2016

1. Introduction

Optimal design is always of great interest to engineers and scientists. More specifically, in the process of engineering design, when all the boundary conditions, aesthetic requirements and other kinds of restrictions are specified, engineers need to design the topology and geometry of an object to achieve its engineering properties and reduce its cost in production.

We focus on topology optimization in this thesis. Different from shape optimization, whose main task is to find the optimum boundary layout or form of a structure, topology optimization owns a broader definition and it allows the change of material distribution in the bulk of a structure. Both shape and topology optimization are constrained optimization problems, yet they are distinct from the standard constrained optimization problems, because PDE constraints are involved, which is in a form of equilibrium. This feature increases the complexity of an optimization problem, since a PDE constraint is expensive to evaluate for each iteration in the course of optimization.

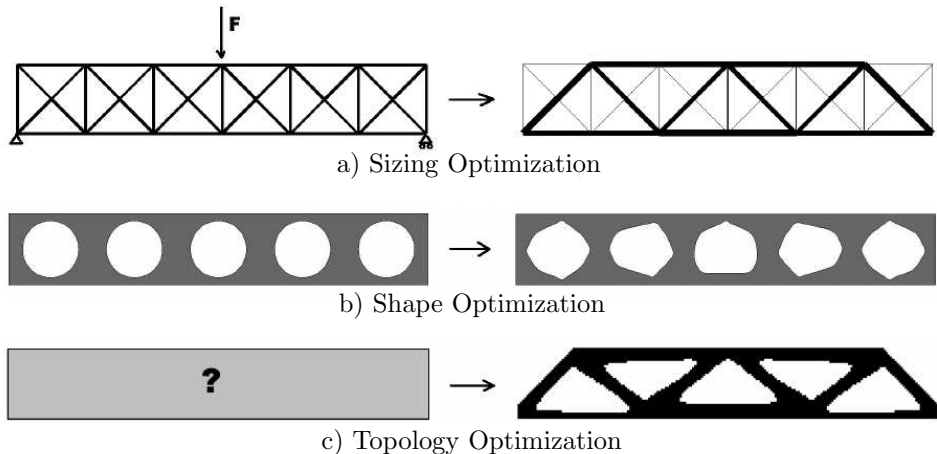


Figure 1: Comparison of different optimization problems in structural design.

One of the most popular approaches to topology optimization is called SIMP (Simplified Isotropic Material with Penalization), which goes back to Bendsøe M.P. and Sigmund O. [12]. It introduces a power function to penalize the intermediate state between material and void. Simple as its concept is, it gives rise to problems such as mesh-dependence, checkerboard pattern, local optimum and no sharp interface between material and void. However, specific techniques are proposed to handle these issues. Due to the relative maturity of this method, many commercial tools implement this method as a standard approach [5] [49].

Parallelly, ESO type methods (Evolutionary Structural Optimization) were proposed and grow to be another popular approach. It follows the intuitive idea that *weak* parts of a structure are to be removed. To determine whether an element is *weak* or not, a sensitivity number is employed, which is based on a sensitivity analysis. Nevertheless, the criterion using sensitivity number should prevent the optimization process falling into a local optimum or non-optimum. This led to the development of the BESO method (Bidirectional Evolutionary Structural Optimization), and other techniques such as soft kill. In [28] the ESO method is shown to be inefficient and always ends in local optimum. Hence BESO is always preferred in practice. After modification and improvement, the

BESO method has already become a strong tool for structural design and contributed to some applications in Civil Engineering [48]. A review paper by the proposer of ESO/BESO method summarizes the techniques and improvement of this method [34].

The above two methods concern mainly the solid part of a structure. From the aspect of the evolution of the material-void or the material-material interface, the level set method and phase field method come into play. The level set method was at first used to characterize the complex boundary of an object and soon gained popularity in many other engineering fields. Based on the Hamilton-Jacobi equation and sensitivity analysis, the material interface can be driven to an optimal state. Initially this method was developed to solve shape optimization problems [2]. The association with the topological derivative broadens its usage in topology optimization. This method was researched very actively in recent years. The review paper [27] lists some variants of the level set method and analyzes their features. Compared with the level set method, the phase field method takes a different approach, i.e. defining a diffuse interface. The evolution of interface is driven by the Allen-Cahn equation or the Cahn-Hilliard equation. Different formulations were proposed in implementation. In Takezawa's approach [70], the result of sensitivity analysis is input in the source term of a diffusion reaction equation, while in Wallin's approach the sensitivity drives the evolution directly. Details of the phase field method will be discussed in a later chapter of this thesis.

In the present thesis, phase field methods are investigated and compared. Their potential in standard compliance optimization problems, thermomechanical optimization problems and coupled field unit cell optimization problems are explored. Our formulation of optimization problems is inspired by [70], [73] and [40].

The thesis is organized as follows: Chapter 2 introduces the basics of topology optimization, Chapter 3 presents two phase field approaches, Chapter 4 gives our generalized formulation and the topology optimization algorithm, numerical results are demonstrated in Chapter 5, comments and summaries of the whole thesis are stated in the last Chapter.

2. Basics of Topology Optimization

The pioneer work in topology optimization goes back to Bendsøe M.P. and Kikuchi N. [11] who incorporated homogenization technique into topology optimization to characterize material properties. Since the proposal of the SIMP method by Sigmund and coauthors [67], the field of topology optimization has attracted researchers from Mechanics and Applied Mathematics. The development of SIMP method is greatly influenced by the emergence of various techniques, such as regularization and filtering. Besides, the educational article [62], which presents the key concepts and implementation details of the topology optimization in a compact way, introduces SIMP method to large audience in academia as well as industry. New methods tackle the problem from a different angle, i.e. the evolution of interface. Level set methods and phase field methods fall into this category.

In this chapter the basic formulation of topology optimization problems is introduced. We emphasize that the SIMP method and its techniques have many connections with other methods. For this purpose, the concepts and techniques of SIMP method are reviewed and discussed. Then we approach the topology optimization problem by describing the evolution of interface. Two methods, the level set method and the phase field method are presented. We close this chapter with a brief discussion of some specific issues, i.e. multi objective optimization, manufacture constraints and multiscale optimization.

2.1. Problem Formulation

On a design domain D assume that we have a design variable ρ and our objective function is $F(\mathbf{u}, \rho)$. As constraints we have a volume constraint c , an equilibrium equation $g(\mathbf{u}, \rho)$ depending on the design variable (a PDE constraint) and constraints for design variable written as an admissible set \mathbb{E}_{ad} . Additional constraints can be added in the problem. With these definitions the topology optimization problem is formulated as (2.1).

$$\begin{aligned} & \min_{\rho} F = F(\mathbf{u}, \rho) \\ \text{subject to } & C_{\text{vol}}(\rho) = \int_D \rho(\mathbf{x}) dV - V_0 \leq 0, \\ & g(\mathbf{u}, \rho) = 0, \\ & \rho \in \mathbb{E}_{ad}. \end{aligned} \tag{2.1}$$

The design variable ρ can be any kinds, the most common ones are size parameters for size optimization, geometry parameters for shape optimization and material density function for topology optimization. Furthermore, the objective function F has a lot of candidates ranging from the ubiquitous compliance objective function to the conversion ratio in piezoelectrical energy harvesting elements [45]. Different from other types of optimization problems, here we always have a partial differential equation as constraint. For the admissible set of a design variable, in SIMP method it can be expressed with bound constraints, i.e. $0 \leq \rho \leq 1$, while in discrete type approaches such as ESO/BESO, the design variable can only be either 0 or 1. Here we present the commonly discussed compliance optimization problem, where the design variable is a material density function

ρ and the concerned PDE constraint is expressed in a weak form.

$$\begin{aligned} \min_{\rho} \quad & F(\mathbf{u}, \rho) = \int_{\partial\Omega} \mathbf{f} \cdot \mathbf{u} \, dS + \int_{\Omega} \mathbf{g} \cdot \mathbf{u} \, dV \\ \text{subject to} \quad & C_{\text{vol}}(\rho) = \int_D \rho(\mathbf{x}) \, dV - V_0 \leq 0, \\ & a_{\rho}(\mathbf{u}, \mathbf{v}) = l_{\rho}(\mathbf{v}), \quad \forall \mathbf{v} \in U, \\ & 0 \leq \rho \leq 1. \end{aligned} \quad (2.2)$$

In the compliance minimization problem, the weak form $a_{\rho}(\mathbf{u}, \mathbf{v}) = l_{\rho}(\mathbf{v})$, $\forall \mathbf{v} \in U$ corresponds to the mechanical equilibrium of a linear elasticity problem written as,

$$\begin{aligned} -\nabla \cdot (\mathbf{C}_{\rho} \boldsymbol{\varepsilon}(\mathbf{u})) &= \mathbf{g} \quad \text{in } \Omega, \\ \mathbf{u} &= \mathbf{0} \quad \text{on } \partial\Omega_D, \\ (\mathbf{C}_{\rho} \boldsymbol{\varepsilon}(\mathbf{u})) \cdot \mathbf{n} &= \mathbf{f} \quad \text{on } \partial\Omega_N. \end{aligned} \quad (2.3)$$

Explicitly we can write the weak form as follows,

$$\int_{\Omega} \boldsymbol{\varepsilon}(\mathbf{u}) : \mathbf{C}_{\rho} : \boldsymbol{\varepsilon}(\mathbf{v}) \, dV = \int_{\partial\Omega_N} \mathbf{f} \cdot \mathbf{v} \, dS + \int_{\Omega} \mathbf{g} \cdot \mathbf{v} \, dV, \quad \forall \mathbf{v} \in U. \quad (2.4)$$

The above formulation is given on the material domain Ω , where we have Dirichlet boundary condition on $\partial\Omega_D$ as well as Neumann boundary condition $\partial\Omega_N$. A sketch of design and material domain is given in Figure 2. In the following sections we review the SIMP method, level set method and phase field method. The essential techniques are shortly discussed for each method.

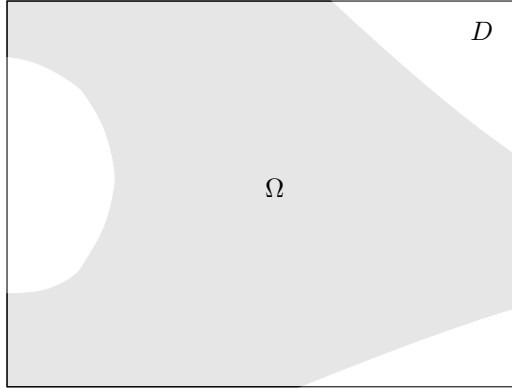


Figure 2: Problem layout. Gray area is for material. The whole rectangular is our design domain.

2.2. SIMP

The SIMP method was conceived by Bendsøe in the 80s [10]. The idea is simply illustrated by its name Solid Isotropic Material with Penalization, where the penalization for the intermediate state is introduced. By intermediate state, we mean $0 < \rho < 1$. When we only consider the interpolation between material and void, we have the following expression

$$\mathbf{C}(\rho) = \rho^p \mathbf{C}^0. \quad (2.5)$$

In this equation, ρ is the material density function, \mathbf{C}^0 is the material parameter and the penalization is realized through a power function with respect to the material density, where the order p is a constant which often takes the value 3. This order p can influence the final pattern to a great extent [12]. Additionally, we have a minimum value ρ_{\min} , so that for void the material parameter is \mathbf{C}_{\min} , namely a fictitious material for void, hence singularity is prevented when solving the PDE constraint on the whole design domain D . It should be noted that the scale function ρ^p is for $\rho \in [0, 1]$, while for other intervals we need to offset the power function accordingly. This scheme can be easily extended to multi-material optimization problems [82]. In comparison with (2.5), many other interpolation schemes have been proposed, many of them account for a material parameter bound such as Hashin-Strikman bound which is shown in [12].

A solution procedure for the implementation of SIMP is outlined in Figure 3. To solve the PDE constraint, we first initialize the design domain with some pattern. Then finite element analysis is applied to the current design pattern, followed by a sensitivity analysis regarding the objective function and the PDE constraint. The purpose of the sensitivity analysis is to obtain the derivative of objective function with respect to the design variable, which is discussed in the following section 2.2.2. An updating step is then carried out with the result of the sensitivity analysis. This step is combined with some specific techniques to get rid of problems such as black-white checkerboard patterns. The loop consisting of the finite element analysis, the sensitivity analysis, and the updating is iterated till a stable and convergent pattern is found. This procedure is demonstrated in the flow chart depicted in Figure 3.

Here we see that the whole scheme is an operator splitting scheme from a more general viewpoint. Normally the whole constraint optimization problem is solved considering all the constraints at once in an iteration. In the current scheme it is realized by splitting the PDE constraint and other normal constraints. The PDE constraint is accounted at the first place, then we generate the sensitivity of F with the result of PDE solution. By observing the input and output variables of each step, this operator splitting can be seen more clearly. Referring Figure 3, we first calculate the field variable \mathbf{u} using ρ , then use \mathbf{u} to obtain $\frac{dF}{d\rho}$, and the next ρ is calculated by using $\frac{dF}{d\rho}$, i.e. $\rho \rightarrow \mathbf{u} \rightarrow \frac{dF}{d\rho} \rightarrow \rho$, where $\frac{dF}{d\rho}$ is the derivative of the objective function obtained in the sensitivity analysis. This scheme is also called Nested Analysis and Design (NAND). We stick to this scheme throughout our work.

A Simultaneous Analysis And Design (SAND) is also possible, see [32], even for non-linear structures [33]. However, only truss examples are considered in both publications due to the enormous degrees of freedom. This method treats field variables also as variables of optimization problem and all the variables (including field variables) are solved in one step in each iteration. It gives a clearer relation between the design variables and field variables and allows the investigation of their respective function spaces under the consideration of Ladyzhenskaya-Babuska-Brezzi condition. In addition, some general constrained optimization tools, e.g. interior point methods, as well as numerical techniques, such as model reduction and domain decomposition, can be exploited (note that we can also use them in the NAND scheme). This direction is still being explored by various scholars. A recent paper [42] clarifies the relation between NAND and SAND. And a general review is given in [6].

Technicality is involved when a practical problem is accounted. Problems such as mesh-

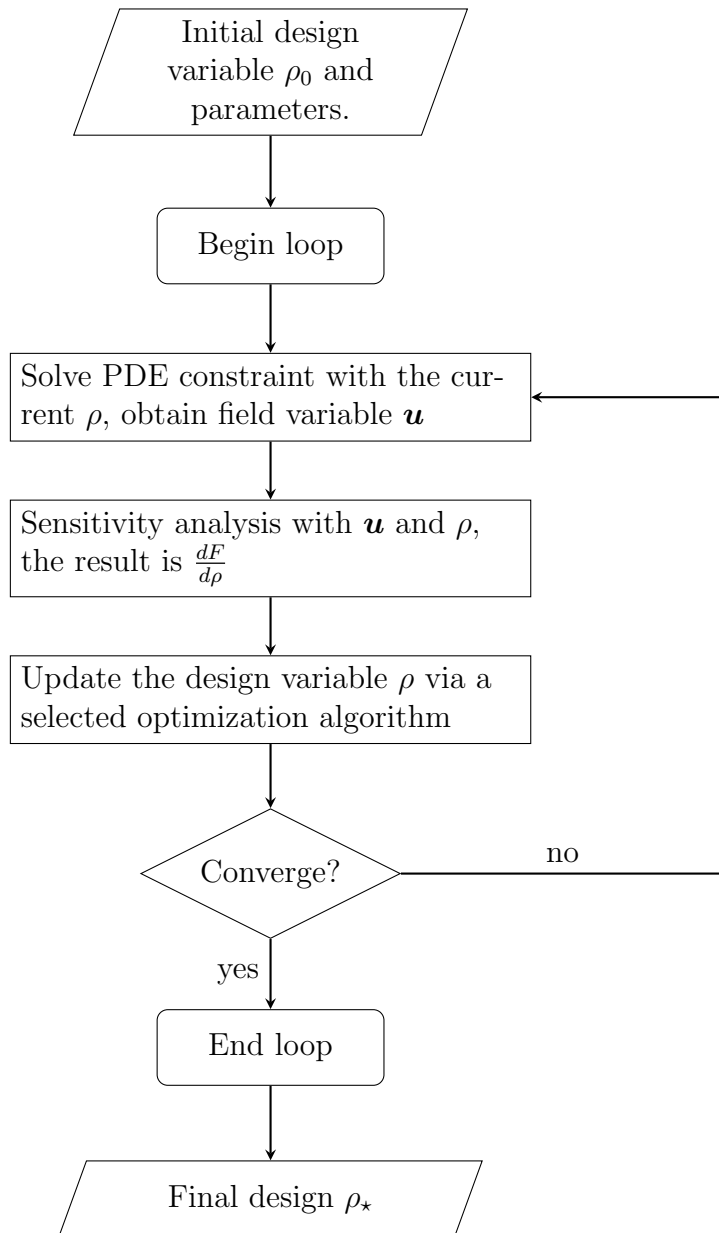


Figure 3: Steps of topology optimization under NAND scheme

dependence, black-white checkerboard patterns, gray area in the optimization result etc. may occur. However, they are overcome by various techniques, such as regularization and filters. These techniques are presented in the section 2.2.3.

2.2.1. Optimality Criteria

The key step in the whole optimization procedure is the update of the design variable ρ , while other steps such as the finite element analysis, and the sensitivity analysis are rather standard. In order to drive the design variable to its optimal state, we need to impose an optimality criterion for the updating of the design variable. This criterion is often stated as Karush-Kuhn-Tucker condition (KKT), which is a necessary condition for finding an optimal solution to the optimization problem [46]. Following the analysis in the book [13], incorporating the PDE constraint into the formulation, we can construct the Lagrangian as,

$$\begin{aligned} \mathcal{L} = F - \{a_\rho(\mathbf{u}, \mathbf{v}) - l_\rho(\mathbf{v})\} + \Lambda \left(\int_{\Omega} \rho(x) dV - V_0 \right) + \\ \int_{\Omega} \lambda^+(\rho(x) - 1) dV + \int_{\Omega} \lambda^-(\rho_{\min} - \rho(x)) dV, \end{aligned} \quad (2.6)$$

where the second term is for the PDE constraint, the third for the volume constraint, and the remaining for the bound constraints of the design variable. It is handled in the first step of the loop in Figure 3. When the PDE constraint is solved, the second term vanishes. The remaining terms give the KKT condition,

$$\nabla_\rho F + \Lambda \nabla_\rho C_{\text{vol}} + \lambda^+ + \lambda^- = 0, \quad (2.7a)$$

$$\int_{\Omega} \rho(x) dV - V_0 \leq 0, \quad \rho(x) - 1 \leq 0, \quad \rho_{\min} - \rho(x) \leq 0, \quad (2.7b)$$

$$\Lambda \geq 0, \quad \lambda^+ \geq 0, \quad \lambda^- \geq 0, \quad (2.7c)$$

$$\Lambda \left(\int_{\Omega} \rho(x) dV - V_0 \right) = 0, \quad \lambda^+(\rho(x) - 1) = 0, \quad \lambda^-(\rho_{\min} - \rho(x)) = 0. \quad (2.7d)$$

An updating scheme according to the KKT system is outlined in the book [13], which is also implemented in the Matlab code [62]. According to [13] the design variable of the next step is calculated by the following formula,

$$\rho_{k+1} = \begin{cases} \max \{(1 - \zeta)\rho_k, \rho_{\min}\} & \text{if } \rho_k B_k^\eta \leq \max \{(1 - \zeta)\rho_k, \rho_{\min}\}, \\ \min \{(1 + \zeta)\rho_k, 1\} & \text{if } \rho_k B_k^\eta \geq \min \{(1 + \zeta)\rho_k, 1\}, \\ \rho_k B_k^\eta & \text{otherwise.} \end{cases} \quad (2.8)$$

with B_k defined as,

$$B_k = -\frac{\nabla_\rho F}{\Lambda \nabla_\rho C_{\text{vol}}}. \quad (2.9)$$

This is a fixed-point algorithm, relating the Lagrange multiplier Λ and the change of strain energy (detailed derivation can be found in [13]). The calculation of the new design variable using the multiplication of the power of B_k lacks physical interpretation, and the choice of parameters such as the move limit parameter ζ and the power parameter η varies

from problem to problem. This updating scheme reminds us of the nonlinear gradient projection method in [46].

Other schemes for the updating design variable can be constructed by using some classical constrained optimization algorithm. [38] discusses and compares the application of sequential quadratic programming (SQP), the method of moving asymptotes (MMA) and optimality criteria (OC) in the topology optimization.

2.2.2. Sensitivity Analysis

In the general formulation of topology optimization problems as in (2.1), the objective function is frequently expressed in terms of the physical state, i.e. the field variable in the PDE constraint. Moreover the PDE constraint $g(\mathbf{u}, \rho)$ is an equation depending on both the field variable \mathbf{u} and the design variable ρ . Therefore the objective function is implicitly a function of the design variable. To calculate the derivative of the objective function with respect to the design variable, we need to perform a sensitivity analysis. A brief introduction about the sensitivity analysis and the calculation of derivative can be found in the chapter 8 of the book [46]. [20] gives a comprehensive discussion on this topic. A recent paper about the second order sensitivity analysis [21] is also very informative.

Basically, there are two approaches for the sensitivity analysis – forward approach and adjoint approach. In the current section, we present the adjoint approach, which is proved to be efficient for topology optimization and used in our work. There are many ways to derive the formula of the adjoint variable. We follow the one given in dolfin-adjoint documentation [26]. Suppose that we have $F(\mathbf{u}, \rho)$ as an objective function, and the PDE constraint is written as $G(\mathbf{u}, \rho) = 0$. We know that the field variable \mathbf{u} depends on ρ . Differentiating the PDE with respect to the design variable ρ leads to,

$$\frac{\partial G}{\partial \mathbf{u}} \frac{d\mathbf{u}}{d\rho} + \frac{\partial G}{\partial \rho} = 0 \Rightarrow \frac{d\mathbf{u}}{d\rho} = - \left(\frac{\partial G}{\partial \mathbf{u}} \right)^{-1} \frac{\partial G}{\partial \rho} \quad (2.10)$$

The substitution of the above formula into the derivative of objective function yields,

$$\begin{aligned} \frac{dF}{d\rho} &= \frac{\partial F}{\partial \mathbf{u}} \frac{d\mathbf{u}}{d\rho} + \frac{\partial F}{\partial \rho} \\ &= - \frac{\partial F}{\partial \mathbf{u}} \left(\frac{\partial G}{\partial \mathbf{u}} \right)^{-1} \frac{\partial G}{\partial \rho} + \frac{\partial F}{\partial \rho} \\ &= -\lambda_u \frac{\partial G}{\partial \rho} + \frac{\partial F}{\partial \rho}, \end{aligned} \quad (2.11)$$

with the adjoint variable λ_u solved by

$$\left(\frac{\partial G}{\partial \mathbf{u}} \right)^* \lambda_u^* = \left(\frac{\partial F}{\partial \mathbf{u}} \right)^* \quad (2.12)$$

Note that $\left(\frac{\partial G}{\partial \mathbf{u}} \right)^*$ is the adjoint operator of bilinear form of the original PDE constraint. Equation (2.12) is called the adjoint problem. If the PDE constraint is linear and its bilinear form is symmetric, the adjoint problem is formulated by just replacing the linear form in the weak form of the PDE constraint by $\left(\frac{\partial F}{\partial \mathbf{u}} \right)^*$.

2.2.3. Filters and Regularization

As mentioned above, many problems might appear in practice. Regularization and filters need to be included in the optimization scheme. The most severe difficulties encountered are mesh-dependence results, black-white checkerboard patterns and local minima. Mesh-dependence means that the solution varies with different meshes, and black-white checkerboard pattern is a pattern with alternating of material and void like a black-white checkerboard, while the local minimum happens when output patterns change with different initial design patterns. The article [68] gives a clear review about each problem and the corresponding strategies to circumvent them. The following table is a summary, which is also presented in the review article.

Table 1: Numerical problems [68].

	Checkerboard	Mesh-dependence	Local minima
Explanation	Inappropriate FE model	Minimal length scale, Nonuniqueness	Nonconvexity
Techniques	1.High order elements 2.Filters 3.Patches 4.Restriction methods	1.Relaxation 2.Perimeter constraint 3.Gradient constraints 4.Mesh-independence filters	Continuation methods

The available filters are listed below with their core expressions as well as their physical interpretation.

Table 2: Filters and regularization techniques.

	Core expression	Interpretation
Perimeter control	$TV(\rho) = \int_D \nabla \rho dx$	Control of total perimeter
Global gradient constraint	$\ \rho\ _{H^1} = (\int_D (\rho^2 + \nabla \rho ^2) dx)^{\frac{1}{2}} \leq M$	H^1 norm of ρ
Local gradient constraint	$ \frac{\partial \rho}{\partial x_i} \leq c$	Pointwise control on derivative
Mesh independent filter	$\widehat{\frac{\partial f}{\partial \rho_k}} = \frac{1}{\rho_k \sum_{i=1}^N \hat{H}_i} \sum_{i=1}^N \hat{H}_i \rho_i \frac{\partial f}{\partial \rho_i}$	Smoothing of sensitivity, add lengthscale
Density filter	$\mathbf{C} = (\rho \star K)^p \mathbf{C}^0$	Filtering via convolution
Patch Method	$\bar{\rho} = \frac{1}{4}(\rho_1 + \rho_2 + \rho_3 + \rho_4)\phi^1 + \bar{v}_2\phi^2 + \bar{v}_3\phi^3$	Superelement, checkerboard-free basis
Intermediate state control	$g(\rho) = \int_D (\rho_u - \rho)(\rho - \rho_l)$ $S(\rho) = \int_D \phi(\cdot, \mathbf{x})\rho(\mathbf{x}) dx$ $P = g \circ S$	Convolution and penalty [18]
Morphology based filter	Dilate, erode, close, and open operator	Image based, eliminate gray area [65]

We realize that the global gradient constraint using L^2 norm is very similar to what we have for the interface energy in a phase field model, and the intermediate penalty constraint is a variant of the double well potential. An available phase field energy is

$$\Phi(\rho) = \int_{\Omega} \left(\frac{1}{\epsilon} \psi(\rho) + \frac{\epsilon}{2} \nabla \rho \cdot \nabla \rho \right) dV. \quad (2.13)$$

2.3. Level Set Method

The level set method is initially a method for representing the surface of an object. It has many applications in various fields [58] such as computer graphics, computational fluid dynamics etc. The idea of this method is to use a level set function to characterize the surface of an object, and to describe the evolution of the surface by specific equations such as Hamilton-Jacobi equation or Eikonal equation [59]. Its application in topology optimization is proposed by Sethian [60] [50] and further developed by Wang, Allaire, etc. They followed a traditional path of level set method, where a Hamilton-Jacobi equation is specified for the evolution. Other researchers use the level set concept to construct filters, such as [9]. Different from above Yamada and coauthors use the level set function to characterize the interface, yet drives the evolution of interface via a diffusion reaction equation [80]. This approach by Yamada and coauthor can be regarded as a transition between level set methods and phase field methods, because of his usage of the level set function and the diffusion reaction equation. A comprehensive review is given in [24].

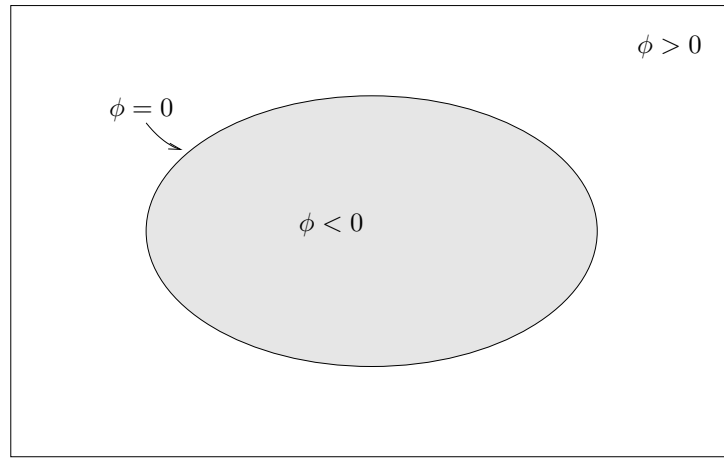


Figure 4: Interface characterization via level set function. $\phi < 0$ for material, $\phi = 0$ for material-void interface, and $\phi > 0$ for void.

The shape representation is realized by a level set function ϕ , which is also our design variable,

$$\begin{cases} \phi < 0 & \text{if } x \in \Omega, \\ \phi = 0 & \text{if } x \in \partial\Omega \cap D, \\ \phi > 0 & \text{if } x \in D \setminus \Omega. \end{cases} \quad (2.14)$$

In the paper of Allaire [3], the ‘‘ersatz material’’ concept is used to map the level set function onto the material properties and no interpolation is involved, which is different from the standard SIMP scheme. After solving the PDE constraint we need to obtain

the derivative of the objective function by the sensitivity analysis. Distinguishing from the SIMP approach, the calculation of objective derivative is based on shape derivative or topological derivative. In the meantime the volume constraint of the problem is addressed with a Lagrange multiplier (fixed value in the [3], updated value with relaxation scheme in [4]) and also included in the shape derivative. This derivative information then goes into the Hamilton-Jacobi equation, specifically in the evolution velocity. Hence the shape derivative or topology derivative and further the evolution velocity takes all the information of the topology optimization into account. The corresponding evolution equation for the level set function is Hamilton-Jacobi equation which is essentially a convection equation,

$$\frac{\partial \phi}{\partial t} + v|\nabla \phi| = 0, \quad (2.15)$$

where the velocity corresponds to the descent direction of the Lagrangian functional, i.e. $v = -\partial_\phi \mathcal{L}(\Omega)$, and $\mathcal{L} = F - \lambda C_{\text{vol}}$.

The above evolution equation can be solved by various numerical schemes, such as finite difference [3], finite element method [1] [4]. One problem about the level set method is that instability occurs in some circumstances and we need to reinitialize the level set function at times. This reinitialization is obtained with the Eikonal equation,

$$\begin{cases} \frac{\partial \phi}{\partial t} + \text{sign}(\phi_0)(|\nabla \phi| - 1) = 0 & \text{in } D \times \mathbb{R}^+, \\ \phi(t=0, x) = \phi_0(x) & \text{in } D. \end{cases} \quad (2.16)$$

However this reinitialization is not compulsory. In [4] reasonable final pattern is obtained without reinitialization.

The level set formulation from Allaire has the advantage of having clear boundary during the simulation and it suits well with shape optimization. Since it cannot create holes in the process of optimization, other terms, i.e. topology derivative should be added to the formulation if a true topology optimization is considered. However, topology derivative will increase the difficulty of problem modeling [47].

This direction of level set method to topology optimization has attracted a lot of researchers, and has progressed with numerous results, see the review paper [27].

2.3.1. Yamada's Approach

Yamada's approach to topology optimization serves as a transition from level set method to phase field method [80]. Different from Allaire's approach he replaces the evolution equation with a diffusion reaction equation. Specific Heaviside functions are applied to the level set function in order to obtain the ersatz material feature from the level set function. The Heaviside operator Yamada and coauthors used is as follows,

$$H_{\text{vol}}(\phi) = \begin{cases} 0 & \phi \leq -1, \\ \frac{1}{2} + \frac{\phi}{2} \left(\frac{15}{16} - \frac{\phi^2}{4} \left(\frac{5}{8} - \frac{3}{64}\phi^2 \right) \right) & -1 < \phi < 1, \\ 1 & \phi \geq 1. \end{cases} \quad (2.17)$$

The volume constraint then becomes,

$$C_{\text{vol}}(\phi) = \int_D H_{\text{vol}}(\phi) dV - V_{\max} \leq 0. \quad (2.18)$$

The diffusion-reaction like evolution behavior is described with the following equation,

$$\begin{cases} \frac{\partial\phi}{\partial t} = K(\phi) \left(\tau L^2 \nabla^2 \phi^2 + C \frac{\partial \mathcal{L}}{\partial \chi_\phi} \right) & \text{in } D, \\ \frac{\partial\phi}{\partial n} = \mathbf{0} & \text{on } \partial D \setminus \partial D_N, \\ \phi = 1 & \text{on } \partial D_N. \end{cases} \quad (2.19)$$

Here we have $K(\phi)$ as a diffusion coefficient, τ as an interface energy parameter, C as a derivative normalizing parameter and L as a characteristic length. The derivative term of the Lagrangian \mathcal{L} with respect to χ_ϕ is a shape derivative same as in Allaire's approach. Yamada used augmented Lagrangian method to enforce the volume constraint, which is elaborated in the educational review paper [51] with Matlab code.

This approach relates with the later proposed phase field formulation of Takezawa et al. [70]. The advantage of this method is that it has a clear interface like the standard level set method discussed above. Moreover hole nucleation can happen during the optimization and the local optimum problem is lessened. One can also see the weakness of this method immediately, i.e. too many parameters (K, τ, C). Searching for proper parameters is always not easy in the course of simulation.

2.4. Phase Field Method

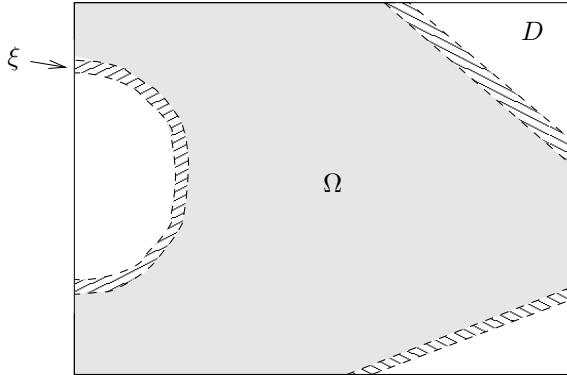


Figure 5: Problem domain. The shaded area ξ is the material-void interface.

The phase field method stands as a method of describing phase separation and phase evolution. The core idea of this method is to employ a specific free energy to drive the evolution of the phases. The simulation of this method always ends in a diffusive interface possessing a certain width, see Figure 5. In this way strong discontinuity is suppressed and problems in computing phase field in the neighborhood of discontinuity is weakened. The basic evolution equation of the phase flow can be different and is based on how we describe the flow. In this section we list the basic evolution equation of the phase field method, and we will discuss this method in detail in the next chapter. We denote ρ as the order parameter in the phase field model, ϵ as the diffusion coefficient, then

$$\rho_t = \epsilon \Delta \rho - \frac{1}{\epsilon} \psi'(\rho), \quad (x, t) \in D \times (0, T]. \quad (2.20)$$

The energy ψ gives a double well potential, e.g. $\psi(\rho) = \frac{1}{4}(\rho^2 - 1)^2$ [22].

2.5. Specific Issues

When it comes to real engineering problems, complicated constraints, various objectives need to be considered. For these problems, specific strategies have been developed.

If multi-objective optimization problem is accounted, we need to clarify the relation between the objectives and the importance of each objective. One possible strategy is to decouple the objectives, multiply them with careful chosen weight parameters and sum them up to form a total objective. Some compliant mechanism problems are multi-objective optimization problems. In [63] [64] the authors defined the compliant synthesis problem for micromechanical system (MEMS). Another representative work for multi-objective optimization is given in [37]. For material design, it is always the case that multiple objectives will arise and we refer to [69] for a standard formulation of this kind.

Multiphysics problems occur frequently in engineering. Many works mentioned above have a multiphysics nature [63] [64] [37]. The essential part of this problem are complex PDE constraints, which is a coupled PDE system. Following the standard procedure of deriving the adjoint problem, it is found out that the adjoint problem for coupled fields can be solved [63]. Other special constraints such as manufacture constraints are also important. For example some part of the domain needs to be fixed or the designed object is connected to an external object. Then how to model such an external object poses a problem. This kind of restriction can be formulated as Dirichlet boundary condition for the evolution step. In manufacturing, we need the bar or thickness of a structure to have a lower bound to meet the precision of manufacturing. This precision requirement can be realized with specific filters which remove thin elements in end results [65] [66] [53].

Multiscale optimization problem is more intricate than the previously discussed ones. The review [78] gives a comprehensive overview on multiscale optimization. There are various types of problems and almost all of them are strongly related with homogenization. Since the computation cost of a complete multiscale optimization problem accounting for microstructures is prohibitive, extra techniques need to be applied, e.g. reduced basis method [77] and parallelization [43] [44]. A more practical viewpoint may be assuming an identical micro structure and decouple scales accordingly [35].

3. Phase Field Approach

The phase field model was firstly introduced to solve solidification problems. Subsequently, it gained popularity in many simulation fields such as fracture modeling [41], and multiphase fluid dynamics [31]. The advantage lies in that phase field models handle interface problems via a certain free energy and end with a diffusive interface. Its application and formulation in continuum mechanics is attributed to Gurtin [30] [25]. Both works formulate the thermodynamics of phase transformation. The derivation in [25] fits especially well in the classical continuum mechanics formulation.

The application of phase field models to topology optimization problems became active recently and is still drawing attentions of many researchers. This direction of topology optimization is pioneered by [25] and followed by [75] [19] [16] [70] [73]. The potential of phase field methods is validated by many numerical results in these papers. Moreover, [15] points out its theoretical convergence and its theoretical relation with other types of approaches to topology optimization. Many practical techniques in realization are demonstrated in these publications.

The core idea of the phase field approach to topology optimization is to add the interface energy as well as the double well potential in an objective function. These two terms correspond with the global gradient constraint or L^2 norm constraint and intermediate state penalty as hinted above in the SIMP filter section, see Table 2. The evolution of phase field is driven by Allen-Cahn equation or Cahn-Hilliard equation.

As for the topology optimization algorithm, we should notice that many of the existing ones are gradient based, no matter whether it is written in a variational form or in a time dependent reaction diffusion problem. Only the first order sensitivity of objective function is gathered for the evolution step. This reveals the possibility of extension with respect to second order sensitivity analysis or an approximation thereof. Constraints are handled in a standard way such as by an augmented Lagrangian method or primal-dual active-set type optimization.

This chapter mainly discusses two approaches after shortly introducing the basics of phase field model. Takezawa's approach makes use of a reaction diffusion equation, while Wallin handles the problem using a variational formulation. Although these two methods have different flavors, they both give some insights on solving the topology optimization problem and lays the foundation of our generalized formulation in the next chapter.

3.1. Interface Representation

In a phase field model we have order parameters characterizing different phases and the interface between phases can be represented in terms of the order parameters. We denote ρ as the order parameter in the current phase field formulation, which is also the design variable. This notation is somewhat different from the standard notation of phase field model which uses ϕ or η .

In Table 3 Ω is the final geometry, Ω_1 , Ω_2 represent two phases, ξ is the diffusive interface between them.

Table 3: Interface representation of level set method and phase representation of phase field method.

Level Set	Phase Field
$\rho = 0 \quad x \in \partial\Omega \cap D$	$\rho = 1 \quad x \in \Omega_1$
$\rho < 0 \quad x \in \Omega$	$0 < \rho < 1 \quad x \in \xi$
$\rho > 0 \quad x \in (D \setminus (\Omega \cup \partial\Omega))$	$\rho = 0 \quad x \in \Omega_2$

3.2. Phase Field Models

In a phase field model the order parameter is driven by a free energy [17]. A typical one is as follows,

$$\Phi(\rho) = \int_{\Omega} \left(\frac{1}{\epsilon} \psi(\rho) + \frac{\epsilon}{2} \nabla \rho \cdot \nabla \rho \right) dV. \quad (3.1)$$

The free energy Φ is also called Ginzburg-Landau energy with the first term representing the bulk free energy density and the second term as an interface energy. The bulk free energy ψ depends on temperature and is often approximated with a polynomial. An available ψ under fixed temperature is the double well potential $\psi(\rho) = \frac{1}{4}(\rho^2 - 1)^2$. We refer to the monograph [52] for an extensive discussion on phase field models.

Taking the variation of this free energy and setting this variational derivative as the evolving direction delivers the Allen-Cahn equation,

$$(Allen-Cahn) \quad \begin{cases} \rho_t = \epsilon \Delta \rho - \frac{1}{\epsilon} \psi'(\rho) & (x, t) \in D \times (0, T] \\ \partial_n \rho|_{\partial\Omega} = 0 \\ \rho|_{t=0} = \rho_0 \end{cases} \quad (3.2)$$

Assumed that the order parameter is locally conserved, combined with the diffusion law a higher order Cahn-Hilliard equation can be derived,

$$(Cahn-Hilliard) \quad \begin{cases} \rho_t = -\Delta \left(\epsilon \Delta \rho - \frac{1}{\epsilon} \psi'(\rho) \right) & (x, t) \in D \times (0, T] \\ \partial_n \rho|_{\partial\Omega} = 0, \quad \partial_n \left(\epsilon \Delta \rho - \frac{1}{\epsilon} \psi'(\rho) \right)|_{\partial\Omega} = 0 \\ \rho|_{t=0} = \rho_0 \end{cases} \quad (3.3)$$

A detailed derivation can be found in [17].

Note that the free energy function (3.1) is related with the Lyapunov functional of these two ordinary differential equations. Further it indicates the asymptotic stability of the result. This properties are presented in [61]. Some numerical analysis is also given in [61].

In topology optimization problems, we usually do not require local conservation. Therefore Allen-Cahn equation is often used. [22] is a general review on phase field models and the applications.

Phase Field Models in Topology Optimization

As discussed and compared in the subsection 2.2.3, the double well potential in the phase field energy serves as a penalization of intermediate state and the interface energy term controls the width of diffuse interface. Hence it is reasonable to use the phase field model in the topology optimization problem and it will eliminate the problems discussed in the subsection 2.2.3.

In the later sections of this chapter and the next chapter, we show that there are in fact two formulations to approach the topology optimization problem using phase field models. One is to use the Allen-Cahn equation, which is basically a reaction diffusion equation, where we input the information of optimization problem in the source term. The other is to use variational formulation such as in [73], where the phase field energy is incorporated in the Lagrangian of the optimization problem.

3.3. Takezawa's Approach

The core evolution equation of Takezawa's approach in [70] is,

$$\frac{\partial \rho}{\partial t} = \kappa \Delta \rho - \frac{\partial \Phi(\rho)}{\partial \rho}. \quad (3.4)$$

The phase field energy $\Phi(\rho)$ is constructed as below,

$$\Phi(\rho) = W(x)w(\rho) + G(x)g(\rho) \quad (3.5)$$

with the definition,

$$w(\rho) = \rho^2(1-\rho)^2, \quad g(\rho) = \rho^3(6\rho^2 - 15\rho + 10). \quad (3.6)$$

The plots of $w(\rho)$ and $g(\rho)$ are shown in Figure 6, and their composition $\Phi(\rho)$ in Figure 7. $W(x)$ corresponds to ϵ in the phase field energy in (3.1) and is chosen as $\frac{1}{4}$, while $G(x)$ determines the direction of evolution and is calculated with the sensitivity of the total Lagrangian,

$$G(x) = \eta \frac{\mathcal{L}'(\rho_{t_1})}{\|\mathcal{L}'(\rho_{t_1})\|}, \quad \text{with } \mathcal{L} = F + \lambda c_{\text{vol}}, \quad (3.7)$$

where $c_{\text{vol}} \leq 0$, $\lambda \geq 0$. The purpose of this construction is twofold, 1. penalize the intermediate states using $w(\rho)$, 2. penalize the evolution direction by multiplying $g(\rho)$. Plugging (3.5) (3.6) (3.7) into (3.4), we have the complete evolution equation,

$$\frac{\partial \rho}{\partial t} = \kappa \Delta \rho + \rho(1-\rho) \left\{ \rho - \frac{1}{2} - 30\eta \frac{\mathcal{L}'(\rho_{t_1})}{\|\mathcal{L}'(\rho_{t_1})\|}(1-\rho)\rho \right\}, \quad \text{for } (t_1 \leq t \leq t_2). \quad (3.8)$$

The procedure of optimization is identical with the one for SIMP. The design variable ρ is calculated using the finite difference method and in order to constrain the design variable in the interval $[0, 1]$ a semi-implicit scheme is proposed,

$$\begin{aligned} \frac{\rho_{i,j}^{n+1} - \rho_{i,j}^n}{\Delta t} &= \kappa \left(\frac{\rho_{i-1,j}^n - 2\rho_{i,j}^n + \rho_{i+1,j}^n}{\Delta x^2} + \frac{\rho_{i,j-1}^n - 2\rho_{i,j}^n + \rho_{i,j+1}^n}{\Delta y^2} \right) \\ &+ \begin{cases} \rho_{i,j}^{n+1}(1 - \rho_{i,j}^n)r(\rho_{i,j}^n) & \text{for } r(\rho_{i,j}^n) \leq 0, \\ \rho_{i,j}^n(1 - \rho_{i,j}^{n+1})r(\rho_{i,j}^n) & \text{for } r(\rho_{i,j}^n) > 0, \end{cases} \end{aligned} \quad (3.9)$$

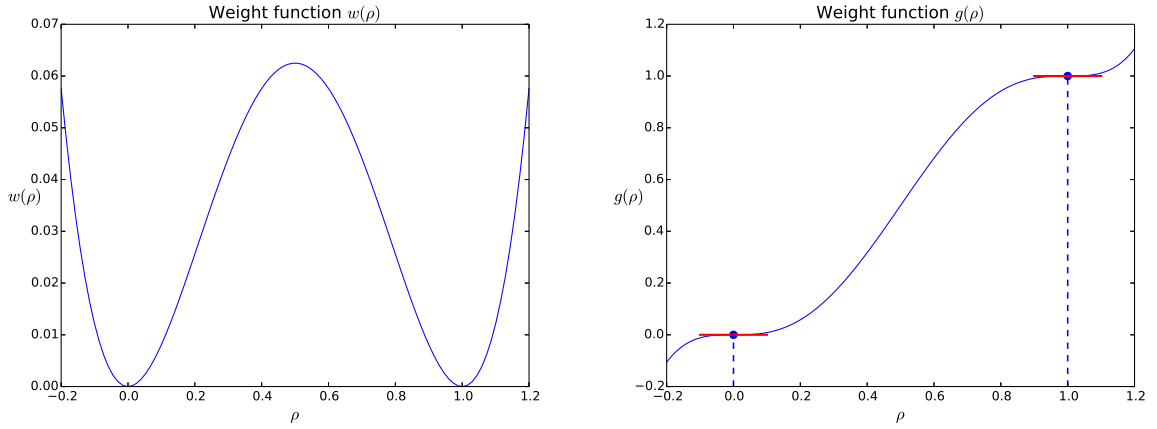


Figure 6: Weight function $w(\rho)$ and $g(\rho)$.

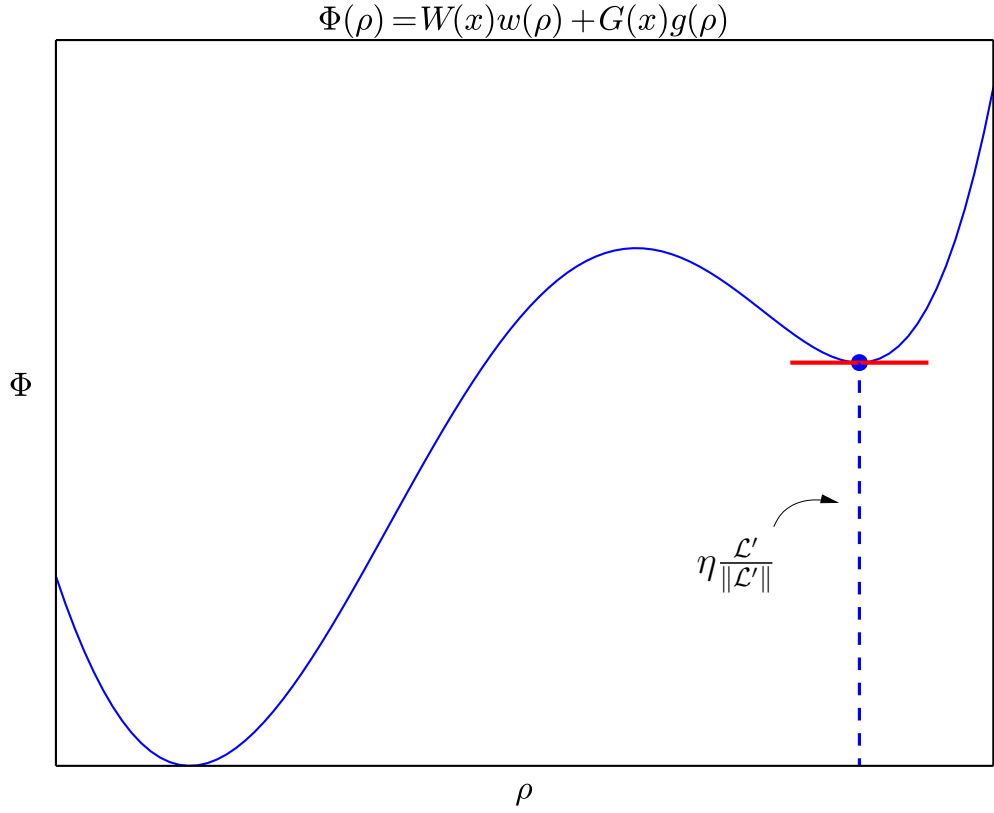


Figure 7: Phase energy $\Phi(\rho)$.

with the following residual

$$r(\rho_{i,j}^n) = \rho_{i,j}^n - \frac{1}{2} - 30\eta \frac{\mathcal{L}'(\rho_{t_1})}{\|\mathcal{L}'(\rho_{t_1})\|} \rho_{i,j}^n (1 - \rho_{i,j}^n). \quad (3.10)$$

As for the volume constraint, we need to update the Lagrange multiplier. This is performed by exploring the KKT system and the shape derivative based on the suggestion

from Allaire [4]. The formula is as follows,

$$\lambda^{n+1} = 0.5 \left(\lambda^n + \frac{\int_{\xi} f(\rho^n) dV}{\int_{\xi} \rho^n dV} \right) + \varepsilon_{\xi} \left(\int_D \rho^n dV - V_0 \right), \quad (3.11)$$

with f being the integrand of the objective functional, i.e. $F = \int_D f(\rho) dV$, the integral domain ξ the diffusive interface, V_0 the prescribed volume, and ε_{ξ} a positive parameter.

We point out that the update of Lagrange multiplier λ is somehow not cleanly defined. It is borrowed from Allaire's level set approach. Nevertheless, the original update in [4] is also a mixture of terms from KKT system. We guess that the first term comes from the solution of KKT system, and the second term stands for a penalty as in the augmented Lagrangian method. Furthermore the introduction of shape derivative in the update makes it harder to adapt the scheme to other kind of objective function. Later we show that the enforcement of constraint can be treated using the standard augmented Lagrangian approach.

To sum up, Takezawa's approach takes many terms and composes them together to achieve topology optimization. Modeling the evolution by taking (3.5) is very technical, but still holds some physical meaning when observing the plot of its belonging terms. This approach shares many features with Yamada's approach [80] such as using reaction diffusion equation as evolution equation. The semi-implicit scheme is efficient, yet needs careful selection of the time step, where the CFL condition applies. The update of Lagrange multiplier is based on the one proposed by Allaire and Pantz [4] and is not well analyzed. Besides that, many parameters have been tuned for the optimization problem. In spite of the listed drawbacks, this method gives reasonable results and some of the difficulties of topology optimization are alleviated. One thing to note is that the evolution of the design variable via a reaction diffusion equation resembles a gradient-based method in optimization.

3.4. Wallin's Approach

Wallin and Ristinmaa formulates the topology optimization problem from a different perspective [73]. The starting point of his approach is to formulate the total Lagrangian considering all the constraints including the PDE constraint, which is analogous with the equation (2.6),

$$\begin{aligned} \mathcal{L}(\rho, \mathbf{u}, \boldsymbol{\lambda}^e, \boldsymbol{\lambda}^t, \lambda^{\rho}) = & \eta F(\rho, \mathbf{u}) + \Phi(\rho) + \int_{\Omega} \boldsymbol{\lambda}^e \cdot (\nabla \cdot \boldsymbol{\sigma}) dV + \\ & \int_{\Omega_t} \boldsymbol{\lambda}^t \cdot (\mathbf{t}_0 - \boldsymbol{\sigma} \cdot \mathbf{n}) + \lambda^{\rho} \left(\int_{\Omega} \rho dV - V_0 \right), \end{aligned} \quad (3.12)$$

where the first term $F(\rho, \mathbf{u})$ is the objective function, the second term $\Phi(\rho)$ is defined as the phase energy, $\nabla \cdot \boldsymbol{\sigma} = \mathbf{0}$ corresponds to PDE constraint with its Neumann boundary condition $\boldsymbol{\sigma} \cdot \mathbf{n} = \mathbf{t}_0$ and the last term represents the volume constraint $\int_{\Omega} \rho dV - V_0 \leq 0$. The constant η in the Lagrangian is a weight parameter for the objective function, and $\boldsymbol{\lambda}^e$, $\boldsymbol{\lambda}^t$, λ^{ρ} are Lagrange multipliers for the corresponding constraints. The variation of this total Lagrangian gives the stationary condition for all the variables. One key step in the derivation is setting $\boldsymbol{\lambda}^e = 2\eta\mathbf{u}$ which is the adjoint variable expressed in an explicit way. This definition is in the context of a compliance optimization problem. After

the substitution of $\boldsymbol{\lambda}^e = 2\eta\mathbf{u}$ and grouping of the variables, the stationary condition is obtained as

$$\frac{1}{\epsilon}\psi_{,\rho} - \epsilon\Delta\rho - 2\eta\frac{g_{,\rho}}{g}w = -\lambda^\rho, \text{ on } D, \quad (3.13)$$

with $g(\rho)$ as a scaling function for material parameter interpolation, cf. (2.5), w as the specific strain energy. The negative of variational derivative of Lagrangian is chosen as the descent direction for the updating step of ρ , namely,

$$\int_\Omega \epsilon\dot{\rho}\xi \, dt = -\frac{\delta\mathcal{L}}{\delta\rho}(\xi). \quad (3.14)$$

We bear in mind that the above equation is written in a variational derivative form. Insertion of the variation of total Lagrangian and the evolution equation for the design parameter ρ reads

$$\epsilon\dot{\rho} = \epsilon\Delta\rho - \frac{1}{\epsilon}\psi_{,\rho} + \eta\boldsymbol{\varepsilon} : \mathbf{C}_{,\rho} : \boldsymbol{\varepsilon} - \lambda^\rho. \quad (3.15)$$

In this formula we have $\psi_{,\rho}$ as the derivative of double well potential, $\mathbf{C}_{,\rho}$ as the derivative of material tangent moduli, and $\boldsymbol{\varepsilon}$ as the linear strain measure. From this derivation, we can see that the variation of the total Lagrangian is obtained first, which is similar with SIMP method, then this variation is applied in an evolution equation as in the derivation of phase field model in [76]. The sensitivity analysis or adjoint problem is avoided by the direct definition $\boldsymbol{\lambda}^e = 2\eta\mathbf{u}$ for the compliance optimization problem.

Solving this evolution equation together with the bound constraint and volume constraint. Wallin et al. employed the Howard's algorithm, which is a policy iteration scheme for the double obstacle problem. Time and mesh size adaptivity are also included in their numerical scheme. The extensions to multi material system and large strain problems are also proposed in other work of Wallin et al., see [74] [72].

In conclusion, Wallin's approach is a variational approach and it has strong connection with the formulation of Allen-Cahn equation, i.e. equation (3.13) is actually Allen-Cahn equation, and by equating (3.15) to zero we recover the stationary condition of (3.13). Finite element method is employed when solving the evolution equation (3.15). The constraints are imposed by Howard's algorithm and can be replaced by other schemes. Although we still have the weight parameter η and phase field parameter ϵ to be specified, the final result patterns show less dependency on the initial inputs. Moreover hole nucleation is attained in the optimization.

4. Numerical Formulation and Implementation

In this chapter we present our optimization scheme. The essential part of our scheme is the time evolution of design variable. Our time evolution scheme stems from Takezawa's approach [70] and Wallin's approach [73]. We reformulate these approaches adding generalized weight parameters respectively. In the first step we compose the total Lagrangian with the objective function, the phase field energy and the constraint. Then either an incremental variational formulation or a formulation via reaction diffusion is carried out. The incremental variational formulation is inspired by [40]. To account for the volume constraint we employ the augmented Lagrangian method [46].

In the first part of this chapter we review the augmented Lagrangian method and motivate for the time evolution of the design variable. Then a topology optimization algorithm is set up and its relevant numerical details are clarified. This is followed by a short presentation of the implementation concepts in FEniCS.

4.1. Augmented Lagrangian Method

The augmented Lagrangian method can enforce both equality constraints and inequality constraints efficiently [46] [29] and it is commonly used in large scale problems. Optimization packages like LANCELOT are heavily based on this method. Here we present the augmented Lagrangian method as a preparation for the later proposed topology optimization algorithm.

A constrained optimization problem can be easily turned into the following form (for other kinds of constraints, we refer to [46] for transformation),

$$\min_{x \in \mathbf{R}^n} f(x) \quad \text{subject to} \quad c_i(x) = 0, \quad i = 1, 2, \dots, m, \quad l \leq x \leq u. \quad (4.1)$$

The equality constraints are then incorporated into the Lagrangian by constructing an augmented Lagrangian as,

$$\mathcal{L}(x, \lambda; \mu) = f(x) - \sum \lambda_i c_i(x) + \frac{\mu}{2} \sum c_i^2(x) \quad (4.2)$$

Denoting λ as a vector of Lagrange multiplier we write the subproblem at the k-th iteration (λ_k and μ_k are the parameters of the k-th iteration) as,

$$\min_x \mathcal{L}(x, \lambda_k; \mu_k) = f(x) - \lambda_k^T c(x) + \frac{\mu_k}{2} \|c(x)\|^2 \quad \text{subject to} \quad l \leq x \leq u. \quad (4.3)$$

Solving this subproblem requires us to make sure that the variable x stays in this interval. Standard algorithms like the active set method, the interior point method, and the gradient projection method can solve this type of problem efficiently [46].

Adding tolerance and scaling parameters we can formulate the problem in an adaptive way as outlined in Algorithm 1. The Algorithm 1 is extracted from the book [46]. We mention that the method for solving subproblem (4.3) can be replaced by other methods such as interior point methods. Although the adaptation of the convergence parameter is heuristic, it can stabilize the optimization. Because the penalty μ_k in the algorithm is always larger than 1 and the convergence parameters ω_k and η_k are always smaller than 1, tolerance is always shrunk at the end of each iteration. However, when the constraint violation is large, the tightening of convergence parameters is eased.

Algorithm 1 Bound Constrained Lagrangian Method [46]

```

Set penalty parameter  $\mu > 0$ , scale factor  $\tau > 1$ ;
Set convergence tolerance  $\eta_*, \omega_* \ll 1$ ;
Choose initial parameters  $\mu_0 \leftarrow 10$ ,  $\omega_0 \leftarrow 1/\mu_0$ ,  $\eta \leftarrow 1/\mu_0^{0.1}$ ;
 $k \leftarrow 0$ ,  $\text{converged} \leftarrow \text{False}$ ,  $x \leftarrow x_0$ ,  $\lambda \leftarrow \lambda_0$ ;
repeat
    Solve the subproblem (4.3) using projected gradient method with tolerance  $\omega_k$ 
    the solution is  $x_k$ ;
    if  $\|c(x_k)\| \leq \eta_k$  then
        (test for convergence)
        if  $\|c(x_k)\| \leq \eta_*$  and tolerance  $\omega_*$  satisfied then
             $x_* \leftarrow x_k$ ,  $\text{converged} \leftarrow \text{True}$ ;
        end if
        (update multipliers, tighten tolerance)
         $\lambda_{k+1} \leftarrow \lambda_k - \mu_k c(x_k)$ ;
         $\mu_{k+1} \leftarrow \mu_k$ ;
         $\eta_{k+1} \leftarrow \eta_k / \mu_{k+1}^{0.9}$ ;
         $\omega_{k+1} \leftarrow \omega_k / \mu_{k+1}$ ;
    else
        (increase penalty, tighten tolerance)
         $\lambda_{k+1} \leftarrow \lambda_k$ ;
         $\mu_{k+1} \leftarrow 100\mu_k$ ;
         $\eta_{k+1} \leftarrow 1/\mu_{k+1}^{0.1}$ ;
         $\omega_{k+1} \leftarrow 1/\mu_{k+1}$ ;
    end if
     $k \leftarrow k + 1$ ;
until  $\text{converged}$ 
 $x_* \leftarrow x_k$ ;

```

4.2. Evolution of Design Variable

The crux of the topology optimization problem is its PDE constraint. We need to enforce the PDE constraint in each iteration in our scheme as in Figure 3. Moreover, the derivative of objective function is calculated through an expensive sensitivity analysis. To avoid frequent evaluation of the PDE constraint and sensitivity analysis, we develop a time evolution updating scheme. Based on the work in [70] and [73], two different formulations with generalized weight parameters are proposed. Because we solve the topology optimization problem only with the first derivative of objective function, the evolution can be regarded as a gradient based search step.

In the following two subsections we present two formulations of the evolution step. One is based on reaction diffusion equation [70], while the other is inspired by the variational approach in [40].

4.2.1. Formulation Using Reaction Diffusion Equation

The comparison of Takezawa's approach [70] and Yamada's approach [80] discussed in the subsection 2.3.1 and the section 3.3 respectively implies that the update of design

variable via a reaction diffusion equation can be reformulated in a general way. We have

$$\dot{\rho} = \eta_\xi \Delta \rho - f_{\text{src}}, \quad (4.4)$$

where η_ξ is a diffusion coefficient, and f_{src} stands for the source term of the reaction diffusion equation.

By supplying different source terms in (4.4), we obtain different governing equations for the evolution of design variable. Normally the source term f_{src} contains the information of optimization problem (objective function and constraints) and the penalization term of intermediate state (can be a double well potential). The followings are candidate source terms obtained from [80] [70] [73].

$$\begin{aligned} & (\text{Yamada [80]}) \quad f_{\text{src}} = -K(\phi)C \frac{\partial \mathcal{L}}{\partial \chi_\phi}, \\ & (\text{Takezawa [70]}) \quad f_{\text{src}} = \frac{\partial \Phi(\rho)}{\partial \rho} = \frac{\partial (W(x)w(\rho) + G(x)g(\rho))}{\partial \rho} \\ & \quad \text{with } G(x) = \eta \frac{\mathcal{L}'(\rho_{t_1})}{\|\mathcal{L}'(\rho_{t_1})\|}, \\ & (\text{Wallin [73]}) \quad f_{\text{src}} = \frac{\partial \mathcal{L}^*}{\partial \rho} \\ & \quad \text{with } \mathcal{L}^* = \eta_F F + \frac{1}{\epsilon} \psi - \lambda c_{\text{vol}}, \end{aligned} \quad (4.5)$$

As indicated in the above source terms f_{src} is composed of objective function, constraints, and a double well potential. We multiply each of them with a weight parameter, then a generalized source term is written as follows

$$f_{\text{src}} = \frac{\partial}{\partial \rho} \left(\eta_F F + \eta_\psi \psi - \sum \lambda_i c_i \right), \quad (4.6)$$

η_F , η_ψ are the corresponding weights. λ_i are the Lagrange multipliers for volume constraints. $\psi(\rho)$ is a double well potential, and c_i is the integrand of a constraint (if this constraint is defined on the whole domain using an integral, namely a volume constraint defined in a form $C_i = \int_D c_i dV$). For the derivative of objective F , $\frac{\partial F}{\partial \rho}$ we mean the local form of sensitivity as in the appendix of [70]. The sensitivity of objective F with respect to ρ is calculated with the PDE constraint via an adjoint approach as in (2.11).

With the constraints $c_i \geq 0$, and the Lagrange multipliers $\lambda_i \geq 0$, the evolution of design variable via a reaction diffusion equation is written in the following box,

solve $\dot{\rho} = \eta_\xi \Delta \rho - f_{\text{src}}$, in D ,

with $f_{\text{src}} = \frac{\partial}{\partial \rho} (\eta_F F + \eta_\psi \psi - \sum \lambda_i c_i)$,

$|\rho| \leq 1$, $c_i \geq 0$.

(4.7)

The solution of the (4.7) is discussed in the subsection 4.3.2.

4.2.2. Incremental Variational Formulation

In [40] the authors used an incremental variational formulation to characterize a time dependent problem. Analogously the time dependent evolution in (4.7) can be transformed into an incremental variational form. First we have an evolution equation as in (3.14),

$$\int_D \dot{\rho} \zeta \, dV = -\frac{\delta \mathcal{L}_{\text{top}}}{\delta \rho}(\zeta). \quad (4.8)$$

We extend the Lagrangian \mathcal{L}_{top} with a “dissipative” term $D(\dot{\rho}) = \frac{1}{2} \int_D \dot{\rho}^2 \, dV$,

$$\Pi(\dot{\rho}, \lambda) = \frac{d\mathcal{L}_{\text{top}}}{dt} + D(\dot{\rho}) \quad (4.9)$$

The Lagrangian \mathcal{L}_{top} above is defined with

$$\mathcal{L}_{\text{top}} = \eta_F F + \eta_\psi \int_D \psi(\rho) \, dV + \eta_\xi \int_D \frac{1}{2} \nabla \rho \cdot \nabla \rho \, dV - \sum \lambda_i C_i \quad (4.10)$$

The variational of (4.9) is

$$\begin{aligned} \frac{\delta \Pi}{\delta \dot{\rho}}(\zeta) &= \frac{\delta}{\delta \dot{\rho}} \left(\frac{d\mathcal{L}_{\text{top}}}{dt} \right)(\zeta) + \frac{\delta D(\dot{\rho})}{\delta \dot{\rho}}(\zeta), \\ &= \frac{\delta \mathcal{L}_{\text{top}}[\dot{\rho}]}{\delta \dot{\rho}}(\zeta) + \int_D \dot{\rho} \zeta \, dV, \\ &= \frac{\delta \mathcal{L}_{\text{top}}}{\delta \rho}(\zeta) + \int_D \dot{\rho} \zeta \, dV. \end{aligned} \quad (4.11)$$

It shows that solving the evolution equation (4.8) is equivalent with the variational principle of (4.9), i.e. the $\delta_{\dot{\rho}} \Pi = 0$.

In the following part we develop an incremental variational principle, where a time step is considered and the variation of $\dot{\rho}$ is replaced with variation of ρ . For $t_k \rightarrow t_{k+1}$ the integration of Π over time yields,

$$\Pi^\tau(\dot{\rho}, \lambda) = \mathcal{L}_{\text{top}} - \mathcal{L}_{\text{top},k} + \int_{t_k}^{t_{k+1}} D(\dot{\rho}) \, dt \quad (4.12)$$

We discretize the dissipative term, then we obtain

$$\Pi^{\text{inc}}(\rho, \lambda) = \mathcal{L}_{\text{top}} - \mathcal{L}_{\text{top},k} + \Delta t D\left(\frac{\rho - \rho_k}{\Delta t}\right), \quad (4.13)$$

whose variation with respect to ρ reads,

$$\delta_\rho \Pi^{\text{inc}}(\rho, \lambda) = 0. \quad (4.14)$$

The constraints are

$$|\rho| \leq 1, \quad C_i \geq 0. \quad (4.15)$$

When $\Delta t \rightarrow 0$, the variation $\delta_{\dot{\rho}}\Pi = 0$ coincides with $\delta_{\rho}\Pi^{\text{inc}}(\rho, \lambda) = 0$. The above analysis is summarized in a box below,

solve $\delta_{\rho}\Pi^{\text{inc}}(\rho, \lambda) = 0$, in D ,

with $\Pi^{\text{inc}}(\rho, \lambda) = \mathcal{L}_{\text{top}} - \mathcal{L}_{\text{top},k} + \Delta t D\left(\frac{\rho - \rho_k}{\Delta t}\right)$,

$$\mathcal{L}_{\text{top}} = \eta_F F + \eta_\psi \int_D \psi \, dV + \eta_\xi \int_D \frac{1}{2} \nabla \rho \cdot \nabla \rho \, dV - \sum \lambda_i C_i,$$

$$|\rho| \leq 1, \quad C_i \geq 0.$$

(4.16)

Referring [46], the formulation above can be regarded as a damped formulation with a damping term defined by $D(\dot{\rho})$.

The above problem in the box (4.16) is shown in the following subsection 4.3.2, where we solve it together with an augmented term from augmented Lagrangian method.

4.2.3. Comparison of Formulations

The relation of the two formulations is revealed in the derivation below. In these two formulation the terms with the same weight corresponds with each other and the rate term $\dot{\rho}$ corresponds with the dissipative term $D(\dot{\rho})$, e.g.

$$\dot{\rho} \leftrightarrow \Delta t D\left(\frac{\rho - \rho_k}{\Delta t}\right), \quad \eta_\xi \Delta \rho \leftrightarrow \eta_\xi \int_D \frac{1}{2} \nabla \rho \cdot \nabla \rho \, dV$$

The difference between (4.7) and (4.16) is also obvious. The reaction diffusion equation is in a strong form at each domain point, while the variation of Π corresponds with a weak form. Hence in the reaction diffusion equation, we have f_{src} as a local expression and the derivative for obtaining f_{src} gives a value at each local point. This leads to our definition of local form of sensitivity (F is always a global quantity defined with a integral), which we refer to the appendix of [70]. On the other hand the terms of Π^{inc} are expressed with global quantities defined as an integral over the whole domain D . In our notation system we have the lowercase character for the local variable and the uppercase character for the global ones. One to one (local to global) pairs can be made for two formulations. An example of this local to global pair is the volume constraint. Denoting V_{frac} as a constant representing the volume fraction, we have

$$c_{\text{vol}} = \rho - V_{\text{frac}} \leftrightarrow C_{\text{vol}} = \int_D (\rho - V_{\text{frac}}) \, dV.$$

We can construct f_{src} and \mathcal{L}_{top} in (4.7) and (4.16) in two different ways according to [70] [73]. We denote TK10 for the source term and Lagrangian from [70] and WL13 for [73]. The weight parameters for each terms are compared in Table 4.

In Table 4 the other term in TK10 is expressed with the following expressions,

$$G(x) = \eta \frac{\mathcal{L}'(\rho_k)}{\|\mathcal{L}'(\rho_k)\|}, \quad g(\rho) = 6\rho^5 - 20\rho^3 + 30\rho. \quad (4.17)$$

Table 4: Weight parameters for TK10 and WL13.

	η_F	η_ξ	η_ψ	Other
TK10	0	Const.	$\frac{1}{4}$	$G(x)g(\rho)$
WL13	Const.	$\frac{1}{\eta_\psi}$	η_ψ	-

In $G(x)$ η is a constant weight parameter, and $\mathcal{L}'(\rho_k)$ is the sensitivity of \mathcal{L} evaluated at the previous design variable ρ_k . This sensitivity is defined for each domain point (local form of sensitivity). The Lagrangian functional \mathcal{L} stands for the Lagrangian involving objective function and the volume constraint, i.e. $\mathcal{L} = \eta_F F - \lambda C_{\text{vol}}$. The norm in the denominator is L^2 norm of Lagrangian. We have modified the $g(\rho)$, which is different from [70] and the section 3.3, because our bound constraint is defined with the interval $|\rho| \leq 1$. From the above definition of the extra term in TK10, we have seen that it calculates the evolution direction from the sensitivity of Lagrangian, i.e. \mathcal{L}' and composes it with a weight function $g(\rho)$ coming from phase field models, such as in [17].

With the weight parameters in Table 4, we have the following source terms for the formulation via reaction diffusion equation in (4.7). Supplying the terms into \mathcal{L}_{top} we obtain the Lagrangian for TK10 and WL13. These are summarized in Table 5 and Table 6.

Table 5: Comparison of f_{src} .

TK10	$f_{\text{src}} = \frac{\partial}{\partial \rho} (\eta_\psi \psi + G(x)g(\rho))$
WL13	$f_{\text{src}} = \frac{\partial}{\partial \rho} (\eta_\psi \psi + \eta_F F - \lambda C_{\text{vol}})$

Table 6: Comparison of \mathcal{L}_{top} .

TK10	$\mathcal{L}_{\text{top}} = \eta_\psi \int_D \psi dV + \eta_\xi \int_D \frac{1}{2} \nabla \rho \cdot \nabla \rho dV + \int_D G(x)g(\rho) dV$
WL13	$\mathcal{L}_{\text{top}} = \eta_\psi \int_D \psi dV + \frac{1}{\eta_\psi} \int_D \frac{1}{2} \nabla \rho \cdot \nabla \rho dV + \eta_F F - \lambda C_{\text{vol}}$

In the comparison of f_{src} , the definition is slightly different from [70]. We use our notation here, and the term $\eta_\psi \psi$ corresponds with the term $W(x)w(\rho)$. The comparison of λ (Lagrange multipliers) for TK10 and WL13 are not discussed here, for they are updated according to a selected updating scheme. The numerical results according to TK10 and WL13 are presented in the next chapter. A detailed comparison of TK10 and WL13 is given in the appendix A.

4.3. Topology Optimization with Augmented Lagrangian Method

In this section we combine the concepts of augmented Lagrangian method in the section 4.1 and the evolution formulation in the section 4.2 together to solve our topology optimization problem.

4.3.1. Topology Optimization Algorithm

For the general topology optimization problem presented in (2.1), we have three different kinds of constraints, i.e. PDE constraint, volume constraint, and bound constraints. Referring to the flowchart in Figure 3, we enforce these constraints separately. At first the PDE constraint is evaluated with finite element analysis. After solving the adjoint problem and calculation of the derivative of objective function, we solve the evolution problem with the bound and volume constraints. The whole optimization problem is formulated with an augmented Lagrangian and the augmented Lagrangian includes the volume constraint shown below (μ is the penalty parameter),

$$\hat{\mathcal{L}}_{\text{top}}^a = \eta_F F + \eta_\psi \int_D \psi \, dV + \eta_\xi \int_D \frac{1}{2} \nabla \rho \cdot \nabla \rho \, dV - \lambda C_{\text{vol}} + \frac{\mu}{2} C_{\text{vol}}^2, \quad |\rho| \leq 1. \quad (4.18)$$

When we solve the evolution equation using the incremental variational formulation, we only calculate the first order sensitivity of the objective function F , which means we have the following approximation,

$$\mathcal{L}_{\text{top}}^a = \eta_F \left(F_k + \left. \frac{\partial F}{\partial \rho} \right|_{\rho_k} (\rho - \rho_k) \right) + \eta_\psi \int_D \psi \, dV + \eta_\xi \int_D \frac{1}{2} \nabla \rho \cdot \nabla \rho \, dV - \lambda C_{\text{vol}} + \frac{\mu}{2} C_{\text{vol}}^2. \quad (4.19)$$

In this expression, the term $\left. \frac{\partial F}{\partial \rho} \right|_{\rho_k}$ is the sensitivity of the objective F evaluated at the previous design variable ρ_k .

As demonstrated in the section 4.1 in each iteration there is a subproblem as (4.3). For the incremental variational formulation in box (4.16), we define the incremental functional Π^{inc} as

$$\Pi^{\text{inc}}(\rho, \lambda; \mu) = \mathcal{L}_{\text{top}}^a - \mathcal{L}_{\text{top},k}^a + \Delta t D \left(\frac{\rho - \rho_k}{\Delta t} \right). \quad (4.20)$$

Then for the incremental variational formulation the subproblem for the k-th iteration is as follows,

$$\delta_\rho \Pi^{\text{inc}}(\rho, \lambda_k; \mu) = 0 \quad \text{subject to} \quad |\rho| \leq 1. \quad (4.21)$$

If we formulate the subproblem with a reaction diffusion equation as in (4.7), then we have the following subproblem

$$\dot{\rho} = \eta_\xi \Delta \rho - f_{\text{src},k} \quad \text{with } |\rho| \leq 1, \quad (4.22)$$

where the source term f_{src} is augmented with a penalty term, namely,

$$f_{\text{src},k} = \left. \frac{\partial}{\partial \rho} \right|_{\rho_k} \left(\eta_F F + \eta_\psi \psi - \lambda c_{\text{vol}} + \frac{\mu}{2} c_{\text{vol}}^2 \right). \quad (4.23)$$

The source term $f_{\text{src},k}$ is evaluated at the previous design variable ρ_k . We refer to Table 5 for more specific expressions.

Additionally the sensitivity of objective F with respect to ρ , i.e. the derivative of objective F is calculated via a sensitivity analysis. This step is accomplished with solving

an adjoint problem, which we presented above in the subsection 2.2.2. If the subproblem via reaction diffusion equation is solved, this sensitivity means a local form of sensitivity as shown before. The derivative of objective F is also evaluated at the previous step ρ_k .

The whole algorithm is summarized in the box Algorithm 2. The adaptation of convergence parameters are not carried out in Algorithm 2 as in Algorithm 1

Algorithm 2 Topology Optimization with augmented Lagrangian method

```

Set material parameters, geometry parameters;
Set weight  $\eta_F, \eta_\psi, \eta_\xi$  in (4.16) or (4.7), and time step  $\Delta t$ , penalty parameter  $\eta$ ;
 $k \leftarrow 0$ , converged  $\leftarrow \text{False}$ ,  $\rho \leftarrow \rho_0$ ,  $\lambda \leftarrow \lambda_0$ ;
repeat
    Solve PDE constraint, obtain  $\mathbf{u}$ ;
    Sensitivity analysis, obtain  $\frac{dF}{d\rho}$ ;
    Solve the subproblem (4.21) or (4.22), obtain  $\rho_k$ ;
     $\rho_{k+1} \leftarrow \rho_k$ ;
     $\lambda_{k+1} \leftarrow \lambda_k - \mu c(\rho_{k+1})$ ;
     $k \leftarrow k + 1$ ;
until converged
 $\rho_* \leftarrow \rho_k$ ;

```

4.3.2. Numerical Solution of Subproblem

In this subsection we discuss about how to solve the subproblem (4.21) and (4.22) numerically. There are two differences between the evolution equations and the subproblems. One is the penalty term in terms of the volume constraint, e.g. in (4.21) there is an extra term $\frac{\mu}{2}C_{\text{vol}}^2$ compared with the Lagrangian in (4.16). The other is the linearization of the objective function F . We only consider the first order sensitivity when solving (4.21) and (4.22).

A nonlinear solver can be applied when solving (4.21). We use the SNES solver from PETSc package [7]. Supplying the SNES solver with a proper nonlinear equation and its derivative is needed. The nonlinear equation is $\delta_\rho \Pi^{\text{inc}} = 0$. We employ the symbolic system in FEniCS to obtain the derivative of other terms. Since the symbolic system (UFL interface) in FEniCS cannot handle the derivative of the square of an integral effectively, we approximate the second derivative of the penalty term $\frac{\mu}{2}C_{\text{vol}}^2$ with a mass matrix in our implementation.

For (4.22), we discretize it with an implicit time scheme and express it in a weak form. The following equation is derived,

$$\int_D \frac{\rho - \rho_k}{\Delta t} \zeta \, dV = - \int_D \eta_\xi \nabla \rho \cdot \nabla \zeta \, dV - \int_D f_{\text{src},k} \zeta \, dV, \quad \forall \zeta \in U. \quad (4.24)$$

The above equation (4.24) is solved by a standard finite element method. The source term $f_{\text{src},k}$ is evaluated at the previous design variable ρ_k , where the derivative of objective F is the local form of sensitivity as mentioned before. After solving the evolution, we cut the design variable to enforce the bound constraint $|\rho| \leq 1$. The cut operation is carried

out simply by the following expression,

$$\rho = \begin{cases} 1 & \text{if } \rho \geq 1, \\ \rho & \text{if } -1 < \rho < 1, \\ -1 & \text{if } \rho \leq -1. \end{cases} \quad (4.25)$$

Comparing two solution method to the subproblems (4.21) and (4.22), it is clear to see that the source term f_{src} is evaluated at ρ_k , while the terms in \mathcal{L}_{src} in (4.22) is given with the current design variable ρ . This is summarized in the tables below (Table 7 and Table 8).

Table 7: Dependency of design variable in solving reaction diffusion equation.

$\int_D \left(\frac{\rho - \rho_k}{\Delta t}\right) \zeta dV$	$\int_D \eta_\xi \nabla \rho \cdot \nabla \zeta dV$	$\int_D f_{\text{src},k} \zeta dV$
ρ, ρ_k	ρ	ρ_k

Table 8: Dependency of design variable in solving incremental variational formulation.

$\Delta t D \left(\frac{\rho - \rho_k}{\Delta t}\right)$	$\eta_F F$	$\eta_\psi \int_D \psi dV$	$\eta_\xi \int_D \frac{1}{2} \nabla \rho \cdot \nabla \rho dV$	$-\lambda C_{\text{vol}} + \frac{\mu}{2} C_{\text{vol}}^2$
ρ, ρ_k	ρ_k	ρ	ρ	ρ

4.3.3. Choice of Parameters

Both of the proposed formulations have many parameters. Besides time step and Lagrange multiplier, we have a weight parameter for each term in the formulation. For supplying the weight parameters a natural idea is to make the evolution equation dimensionless and let their contribution to the extended Lagrangian at the same level. Our attempt is to compute the norm of the gradient of the objective function and choose a weight for it such that the norm is in the same order with other terms, e.g. volume constraint term.

We refer [70] and [80] to realize our normalization. The expression for the normalization is

$$\left\| \frac{\partial \eta_F F}{\partial \rho} \right\|_{L^2} \sim \left\| \frac{\partial \lambda c_{\text{vol}}}{\partial \rho} \right\|_{L^2}. \quad (4.26)$$

Note that the L^2 norm is used here. It is important to note that the objective weight calculated above only gives a recommended value, and sometimes it does not work.

The choice of the weight parameters is an important issue in topology optimization. It affects the final design pattern as well as the convergence speed. Later we present plenty of numerical examples for different parameters.

Other parameters besides the weight parameters are time step Δt and the augmented Lagrangian parameter λ, μ . For time step an adaptive scheme is helpful as discussed in

[8]. Because of the semi-implicit character of our time stepping schemes, we select the time step calculated from Courant-Friedrichs-Lowy condition (CFL) as a reference time step. If we have a structured mesh, with element size Δx and Δy in each direction, then

$$\kappa \left(\frac{\Delta t}{\Delta x^2} + \frac{\Delta t}{\Delta y^2} \right) \leq \frac{1}{2}, \quad (4.27)$$

where κ is the weight of interface energy. According to the theory of augmented Lagrangian method in [46], it does not matter how we choose the Lagrange multiplier and the penalty, yet more iterations are needed when the Lagrange multiplier and penalty parameters are not wisely chosen. However when the initial values of the multiplier and the penalty factor are not appropriate, convergence may take a prohibitive amount of time. More comparison of different penalty parameters is presented in the later numerical example chapter.

4.4. Overview of Implementation

4.4.1. FEniCS Framework

FEniCS is an open source finite element framework. The self-explanatory interface makes it very handy for modeling and various linear algebra backends allow us to solve problems efficiently.

The whole program of FEniCS is made up of three major parts. Each part represents one or several functionalities. We express the mathematical model by UFL language. Then with the help of form compiler (FFC), C++ code of the whole model is obtained. The interface between symbolic code and numerical code is called UFC (Unified Form-assembly Code). It can achieve efficient assembling of finite elements [39].

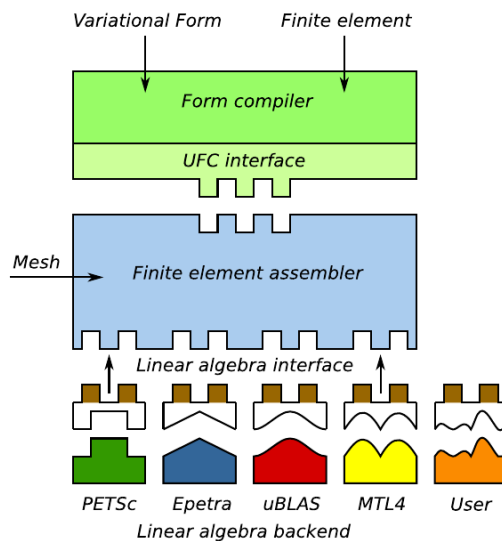


Figure 8: FEniCS Structure.

Numerical algorithms enter after the UFC interface. The main package that carries the numerical algorithm is DOLFIN. DOLFIN's task is to wrap functionalities of each component and their interactions. DOLFIN itself has a C++ as well as a convenient python interface.

Other building blocks are e.g. mshr for geometrical modeling and mesh generation, and FIAT (FInite element Automatic Tabulator) for automatic finite element generation for arbitrary orders. Linear algebra backends provides the possibility of extension. The postprocessing functionalities are also implemented in FEniCS, which allows us to view plots in the course of simulation as well as to write results into files that can be visualized by, e.g. ParaView.

4.4.2. Implementation Concepts

We separate the routines of problem definition and solution scheme and make each functionality as independent as possible. The three main steps in the flowchart Figure 3 correspond to `pde_constr.py`, `adjoint_prob.py` and `optimization_scheme.py`. In this framework we can simply model a topology optimization problem and attribute a method to solve the problem.

For the formulations of evolution we further define four classes:

1. `OptForm`, where all the symbolic and form expressions are stored;
2. `OptProb`, which subclasses the original;
3. `OptSolver`, which controls the link and work flow of evolution including adaptation;
4. `OptScheme`, which forms the unified interface for the approaches.

The solution of a nonlinear problem is achieved by subclassing the `NonlinearProblem` with user defined derivative and Hessian. Regarding solving `NonlinearProblem` we can use either SNES solver or TAO solver in PETSc [7]. These solvers can handle bound constraint efficiently. It is also possible to define `MixedFunctionSpace` in FEniCS. This allows us to solve the KKT system as in (2.7) directly. However this way of solving the optimization problem still needs to be investigated for the current version 2016.1.

5. Numerical Results

In this chapter we present the numerical results. At first, a cantilever compliance problem is solved to validate our formulations and their corresponding numerical scheme. The specific terms used in the validation are constructed according to TK10 and WL13 in the subsection 4.2.3. The contribution of different terms in the formulation is analyzed in the validation. After the validation we compare results of different parameters and thereby give suggestions on the choice of parameters.

Then we discuss the potential of these methods in other problems such as a 3D cantilever compliance optimization problem, a thermomechanical problem and a unit cell optimization problem.

5.1. Cantilever Compliance Problem

5.1.1. 2D Cantilever Beam

The problem in this section is a 2D fixed end cantilever beam subjected to a point load on the right end, see Figure 9. This is a typical benchmark problem suggested in [13]. The result is a Mitchell-type structure [56]. In our problem the length of beam is 2, the height of beam is 1, and we have a load in the middle of right end of our beam. Since applying a point load is not fully provided in FEniCS (`PointSource` works only for scalar field), we approximate this load by a narrow line load on the specified point. The illustration is given below in Figure 9. The load is 0.01. We use an isotropic linear elastic material model. And the corresponding material parameter are set to $E = 1, \nu = 0.3$ (Young's modulus and Poisson's ratio respectively), which have been also used in [70] and [73].

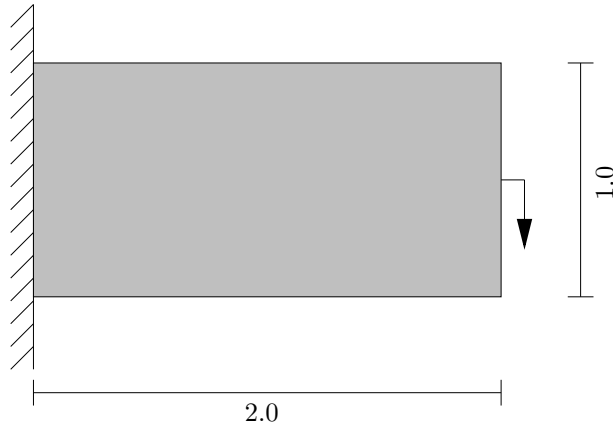


Figure 9: Benchmark problem layout.

The basic compliance optimization problem is described as follows,

$$\begin{aligned} \min_{\rho} \quad & F(\mathbf{u}, \rho) = \int_{\partial\Omega} \mathbf{f} \cdot \mathbf{u} \, dS \\ \text{subject to} \quad & C_{\text{vol}}(\rho) = \int_D \rho(\mathbf{x}) \, dV - V_0 \leq 0, \\ & \int_{\Omega} \boldsymbol{\varepsilon}(\mathbf{u}) : \mathbf{C}_{\rho} : \boldsymbol{\varepsilon}(\mathbf{v}) \, dV = \int_{\partial\Omega_N} \mathbf{f} \cdot \mathbf{v} \, dS, \quad \forall \mathbf{v} \in U, \\ & -1 \leq \rho \leq 1. \end{aligned} \tag{5.1}$$

In this compliance problem there is no body force compared with (2.4) and the force \mathbf{f} is the force acting on the right end. The design variable is restricted in the interval $[-1, 1]$

meaning $\rho = 1$ for material, $\rho = -1$ no material, and other values for intermediate states. Moreover, the material parameters are interpolated with a scale function according to the concept of SIMP method,

$$\mathbf{C}(\rho) = g(\rho)\mathbf{C}^0, \quad \text{with } g(\rho) = \frac{1}{8}(1 + \rho + \rho_{\min})^3, \quad (5.2)$$

where we have 3 as the order parameter in the material interpolation scheme. ρ_{\min} is a parameter to prevent singularity when solving PDE constraint on the whole design domain.

Verification of Methods

Following the discussion in the subsection 4.2.3, we construct a specific source term in the reaction diffusion equation and an augmented Lagrangian for the incremental variational formulation. Our double well potential is expressed with,

$$\psi(\rho) = (\rho^2 - 1)^2 \quad (5.3)$$

Setting weight $\eta_\psi = \frac{1}{4}$, the source term f_{src} , from the following formula provided in the subsection 4.2.3

$$f_{\text{src}} = \frac{\partial}{\partial \rho} (\eta_\psi \psi + G(x)g(\rho))$$

we obtain,

$$(\text{TK10}) \quad f_{\text{src}} = (\rho + 1)(\rho - 1) \left\{ \rho + 30\eta \frac{\mathcal{L}'(\rho_{t_k})}{\|\mathcal{L}'(\rho_{t_k})\|} (\rho + 1)(\rho - 1) \right\} \quad (5.4)$$

In the above formulation we have $\mathcal{L} = \eta_F F - \lambda C_{\text{vol}}$. Note that the \mathcal{L} is slightly different from what is given in the subsection 4.2.3 and in [70]. Here we apply an objective weight η_F for the convenience of our implementation. From the formula of \mathcal{L}_{top} in subsection 4.2.3,

$$\mathcal{L}_{\text{top}} = \frac{1}{\eta_\xi} \int_D \psi \, dV + \eta_\xi \int_D \frac{1}{2} \nabla \rho \cdot \nabla \rho \, dV + \eta_F F - \lambda,$$

we have the augmented Lagrangian for solving the subproblem as in (4.19),

$$(\text{WL13}) \quad \mathcal{L}_{\text{top}}^a = \eta_F \left(F_k + \left. \frac{\partial F}{\partial \rho} \right|_{\rho_k} (\rho - \rho_k) \right) + \frac{1}{\eta_\xi} \int_D \psi \, dV \\ + \eta_\xi \int_D \frac{1}{2} \nabla \rho \cdot \nabla \rho \, dV - \lambda C_{\text{vol}} + \frac{\mu}{2} C_{\text{vol}}^2. \quad (5.5)$$

Note that we use the weight parameter η_ξ rather than η_ψ in the formulation, since it is more convenient for the later discussion.

Referring to [70] and [73] we choose the optimization parameters as in Table 9. Time

Table 9: Parameters for TK10 and WL13.

TK10	$\eta_\xi = 1 \times 10^{-3}$, $\eta = 20$, $\eta_F = 1 \times 10^5$
WL13	$\eta_\xi = 0.02$, $\eta_F = 1 \times 10^5$

step and Lagrange multiplier are set as in Table 10. We mention that the time step Δt

Table 10: Optimization parameters for Algorithm 2.

TK10	$\Delta t = 0.02$	$\lambda^\rho = -40, \mu = 10$
WL13	$\Delta t = 5 \times 10^{-5}$	$\lambda^\rho = -40, \mu = 10$

in the reaction diffusion equation is chosen referring to the time step calculated by CFL condition $\Delta t = 0.1\Delta t_{\text{CFL}}$. And the time step in incremental variational approach is given as in [73]. These time steps in the verification examples are also reference time steps for the later examples.

By substitution of these parameters into our formulation, we have the following weight parameters for the formulation (4.7) and (4.16). The weight of objective in the source term of reaction diffusion equation is only an approximated value because of the normalization of the objective function according to [70]. Through this comparison we find the similarity in the selection of weight parameters in (4.7) and (4.16).

Table 11: Weight parameters in each formulation.

	TK10	WL13
Objective	$\approx 2 \times 10^6$	10^5
Constraint	800	40
Double well	20	50
Interface	0.001	0.02

For the discretization, in the current example a structured triangular linear mesh (100×50 , 10^4 elements) is used in the finite element analysis of PDE constraint as well as in the evolution of the design variable.

As can be observed from Figure 10 and the evolution movie, incremental variational formulation has more oscillation than the formulation using reaction diffusion equation. It may be caused by the inexactness of second order derivative for the nonlinear problem. This inexactness comes from the second derivative of the penalty term, where we approximate it by a mass matrix. Figure 11 shows that both formulations have fluctuation with respect to the volume constraint violation.

Concerning the contribution of terms in the incremental variational formulation, we read from Figure 12 that when the optimization goes to stable state, the $\eta_F F$ term is an order higher than other terms. The stabilization is obtained in after 50 iterations.

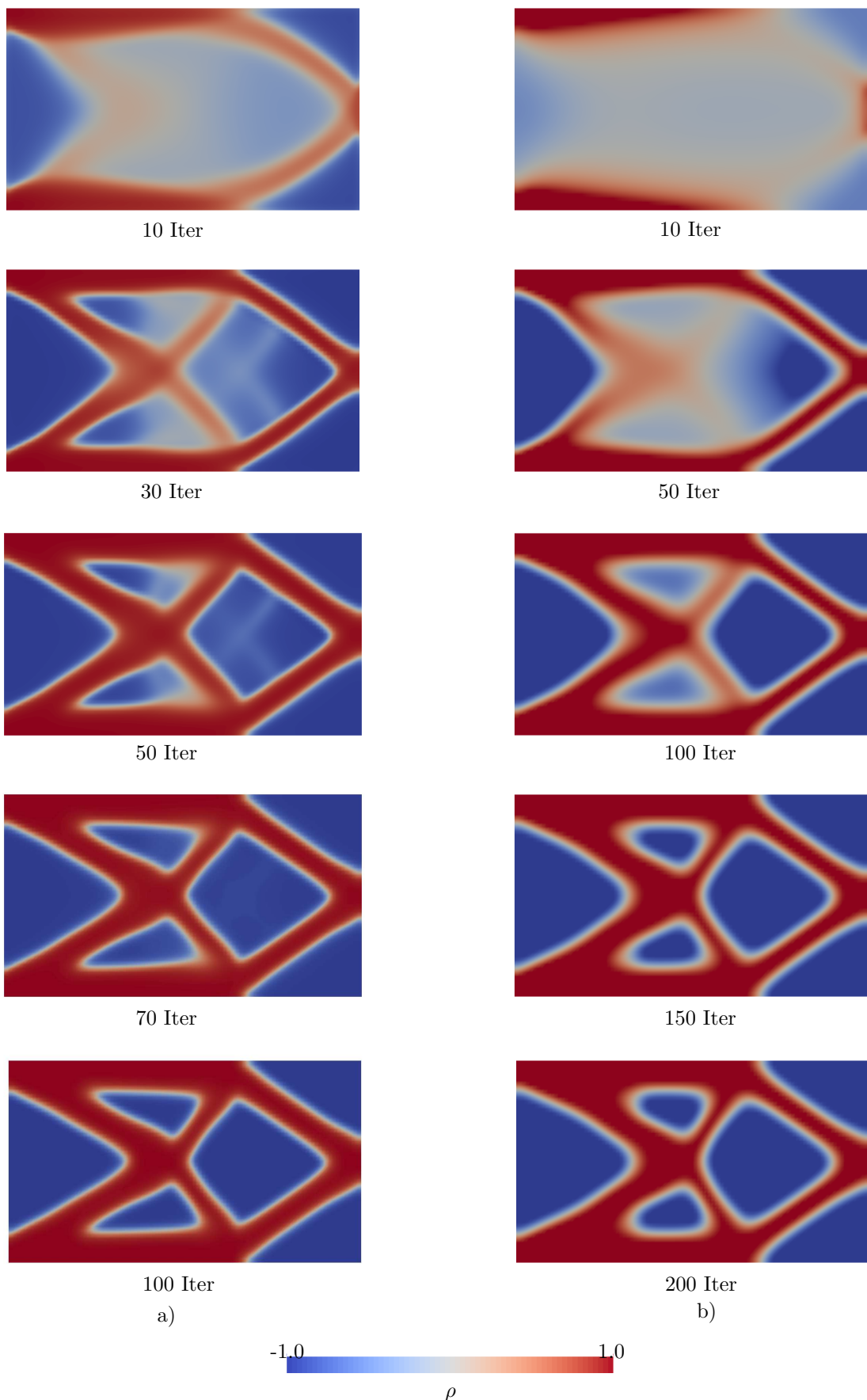


Figure 10: Verification of formulations, a) reaction diffusion equation (TK10), b) incremental variational formulation (WL13).

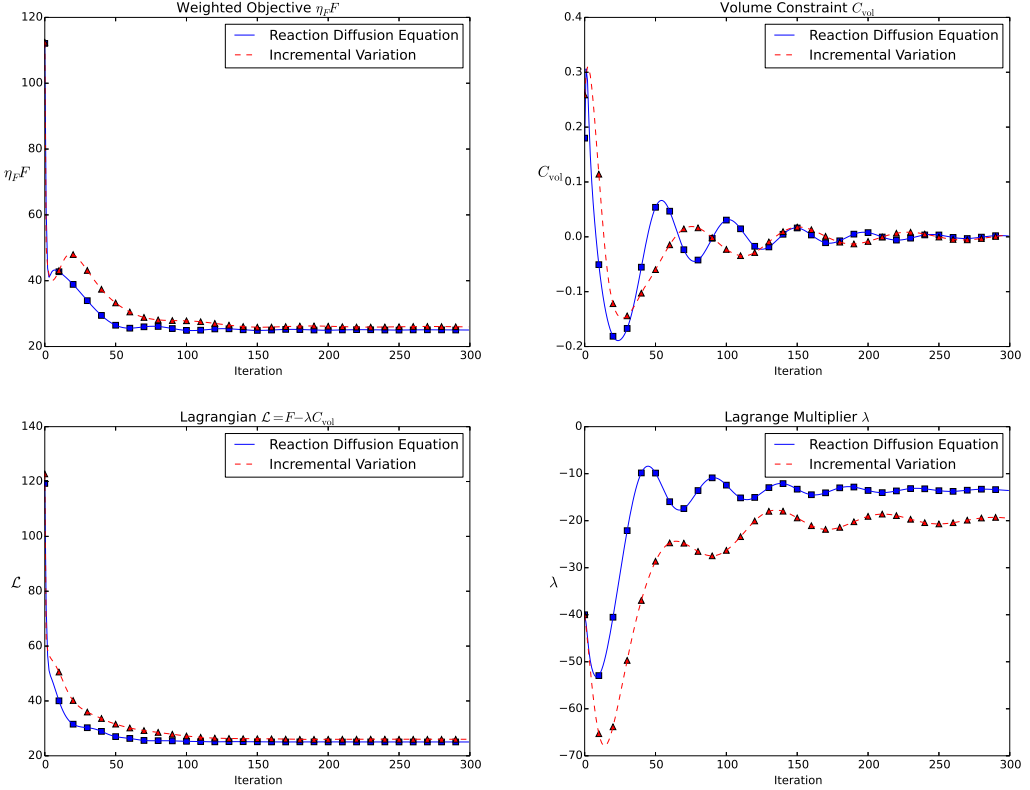


Figure 11: Comparison of formulations, reaction diffusion equation (TK10), and incremental variational formulation (WL13).

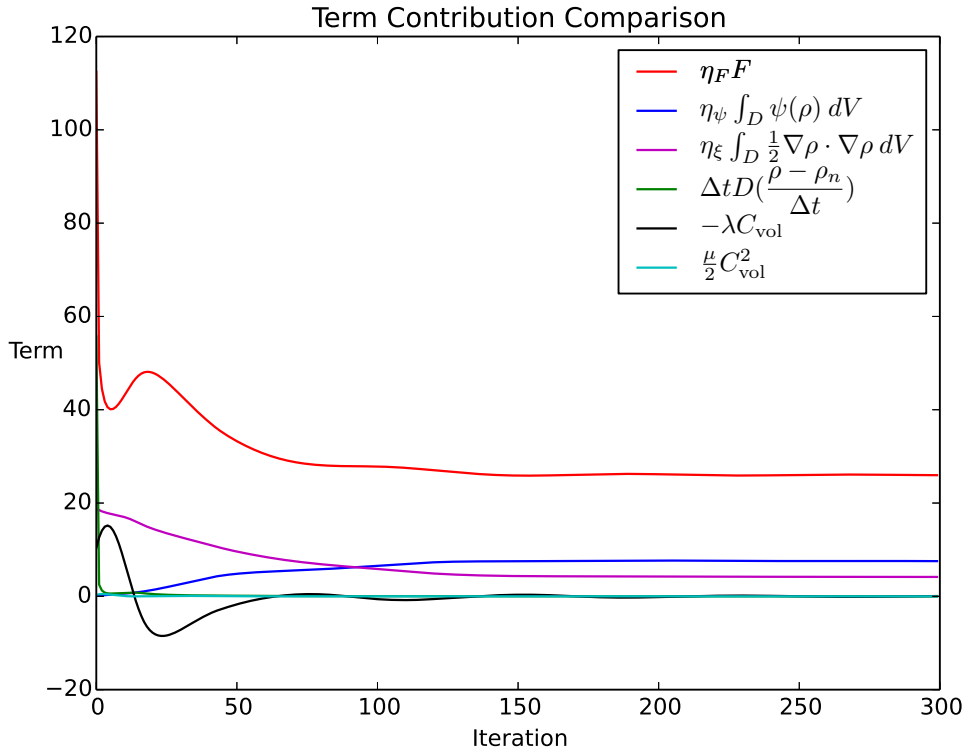


Figure 12: Term contribution in incremental variational formulation (WL13), $\Pi^{\text{inc}} = \eta_F F^{\text{lin}} + \eta_\psi \int_D \psi dV + \eta_\xi \int_D \frac{1}{2} \nabla \rho \cdot \nabla \rho dV - \lambda C_{\text{vol}} + \frac{\mu}{2} C_{\text{vol}}^2 - \mathcal{L}_{\text{top},k} + \Delta t D \left(\frac{\rho - \rho_k}{\Delta t} \right)$.

Different Initial Patterns

We prescribe the final volume as 0.5 of the design domain and show results for different initial patterns. Four different patterns are listed, i.e. a homogeneous pattern with low volume fraction, a homogeneous pattern with high volume fraction, a two hole initial pattern, and a cheese-like pattern. This is for the test of local optimum problem of optimization.

Initial Lagrange multipliers and their penalty parameters are the same across different initial patterns. Optimization parameters for homogeneous initial states are consistent with those in the method verification part except time step is adjusted (for better convergence). For the initial states with holes we need to relax the η_ξ in incremental variational formulation by setting $\eta_\xi = 0.05$. This relaxation means we have a wider diffusive interface and the regularization effect of this term is greater than before.

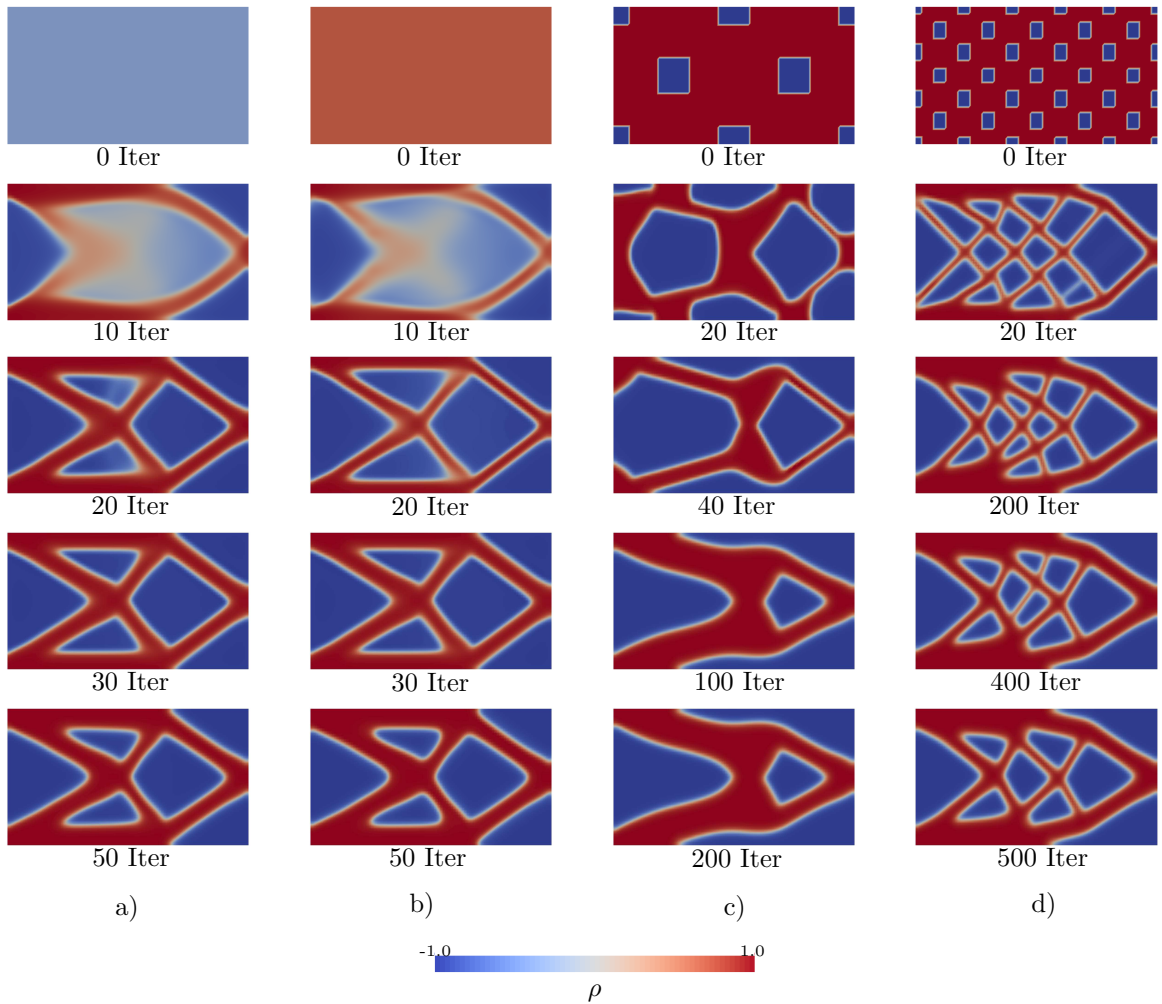


Figure 13: Comparison of different initial states (reaction diffusion equation, TK10), a) homogeneous initial state with -0.4, b) homogeneous initial state with 0.7, c) initial state with two holes, d) homogeneous initial state with many holes.

The result of the formulation using reaction diffusion equation shows: 1. different initial patterns work, homogeneous initial states end in identical solution; 2. holes in initial patterns will end in final patterns with different complexity, and the evolution is related with the initial pattern; 3. holes can be created and removed; 4. iteration times

changed with different initial patterns; the more complex is the initial states, the more iterations we need to find the solution; 5. local minima effect.

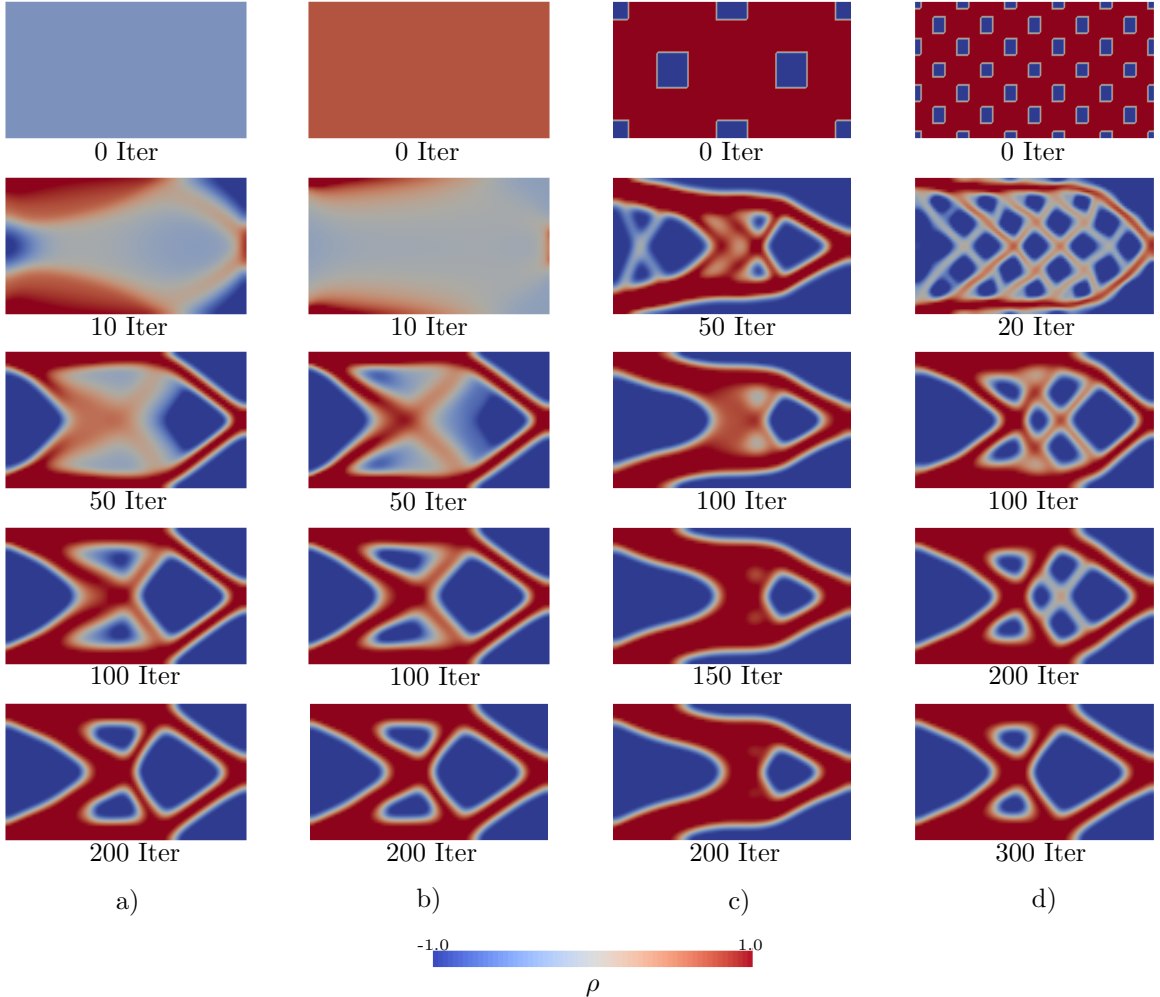


Figure 14: Comparison of different initial states (incremental variational formulation, WL13), a) homogeneous initial state with -0.4 , b) homogeneous initial state with 0.7 , c) initial state with two holes, d) homogeneous initial state with many holes.

For the incremental variational formulation, similar remark can be made as for the reaction diffusion scheme. For the example having many holes, the final state is almost identical with the homogeneous cases. This might be due to high interface energy weight.

Different Meshes

Different meshes are compared in this section. This is especially important for some cases where structured meshes will influence the evolution of design pattern and biased evolution might occur. Optimization on a coarse mesh is useful, when we want to carry out multi-resolution or multi-step optimization [14].

The parameters are the same, only time step is adapted for the formulation using reaction diffusion equation, i.e. for coarse mesh, a smaller time step is used.

Both formulations perform good for different meshes. However for the unstructured mesh, the final pattern has some slight difference with the structured ones, namely the hole on the bottom is slightly smaller. In coarse mesh with the evolution using reaction

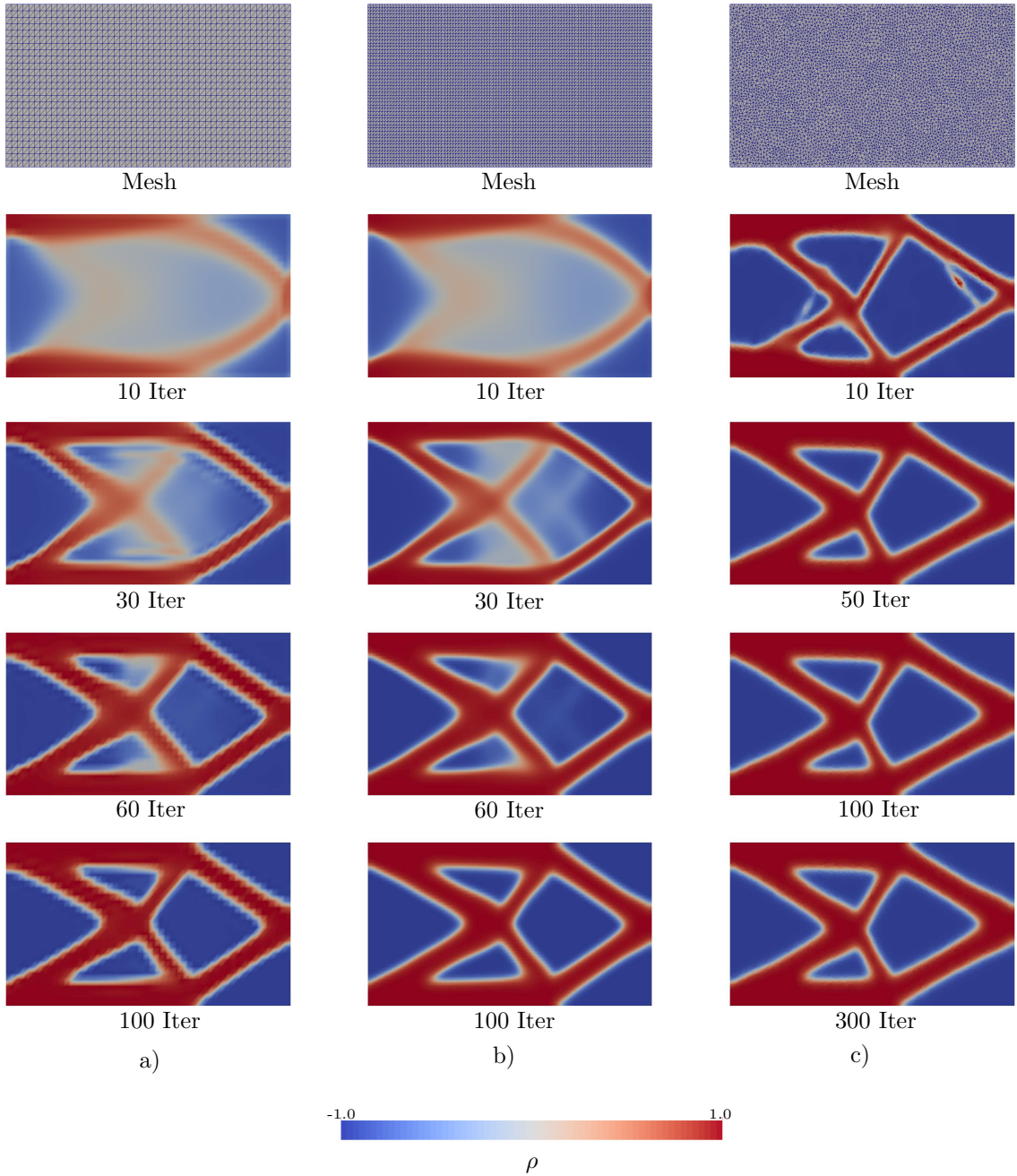


Figure 15: Comparison of different meshes (reaction diffusion equation TK10), initial states are homogeneous with $\rho = 0$, a) coarse structured mesh 25×50 , b) fine structured mesh 50×100 , c) unstructured mesh with approximately the same number of elements 10000 as the fine structured mesh.

diffusion equation, instability is observed in 30 iteration, i.e. checkerboard pattern appear in a small region. In contrary general optimization shows quite consistent results for different meshes, only the pattern is blurred because of the coarsening.

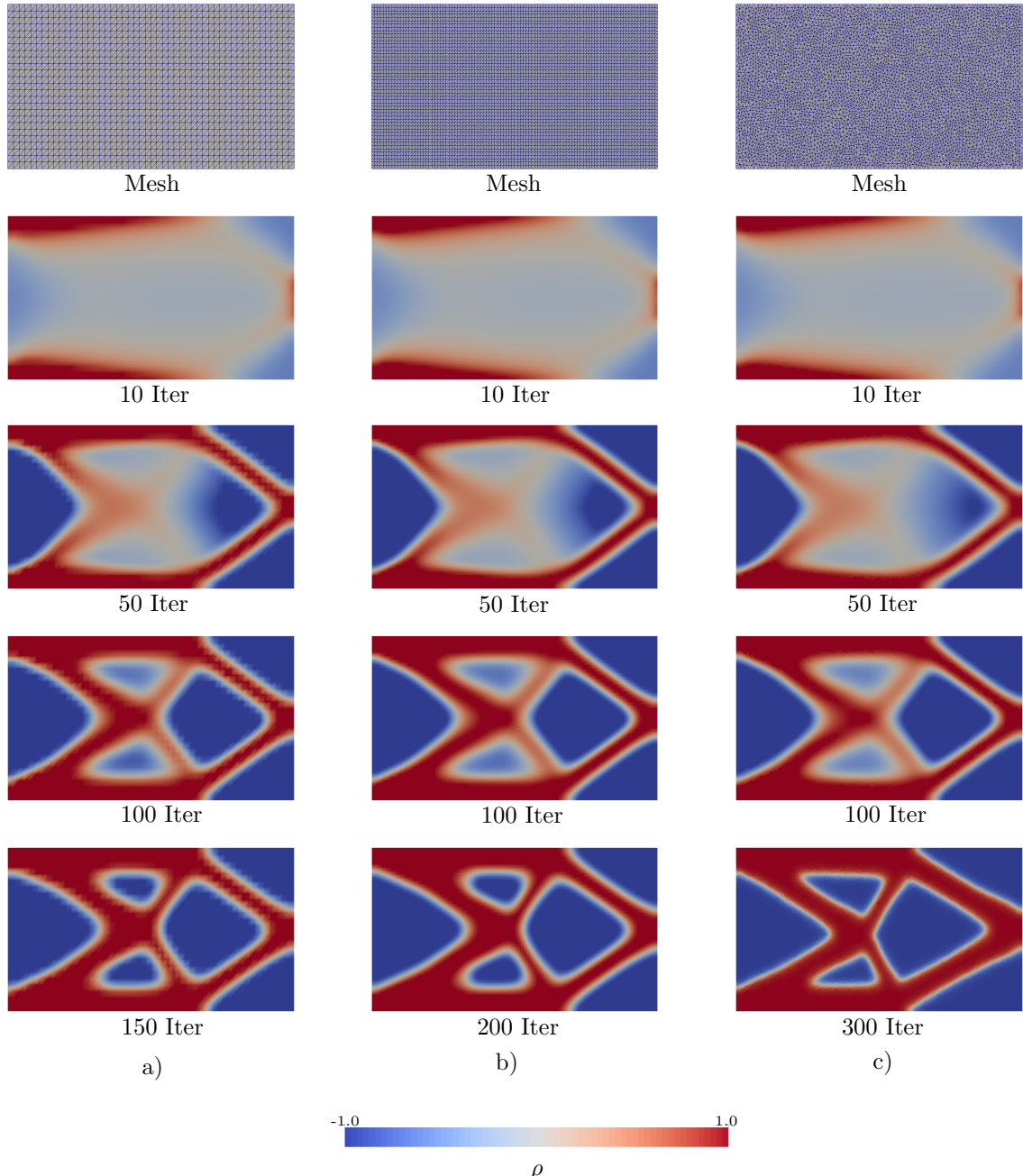


Figure 16: Comparison of different meshes (incremental variational formulation, WL13), initial states are homogeneous with $\rho = 0$, a) coarse structured mesh 25×50 , b) fine structured mesh 50×100 , c) unstructured mesh with approximately the same number of elements 10000 as the fine structured mesh.

Effects of Different Parameters

Extensive comparison of parameters is given in this section. We first discuss the construction of terms from TK10. The varied parameters are η_ξ , η , η_F , μ . In each comparison other parameters are fixed except the compared one. When the result diverges, we reduce the time step accordingly.

We first compare the effect of different diffusion coefficients η_ξ . [15] shows this parameter is related with the diffusive interface width. The smaller η_ξ is, the thinner the interface. All these observations are based on Figure 17.

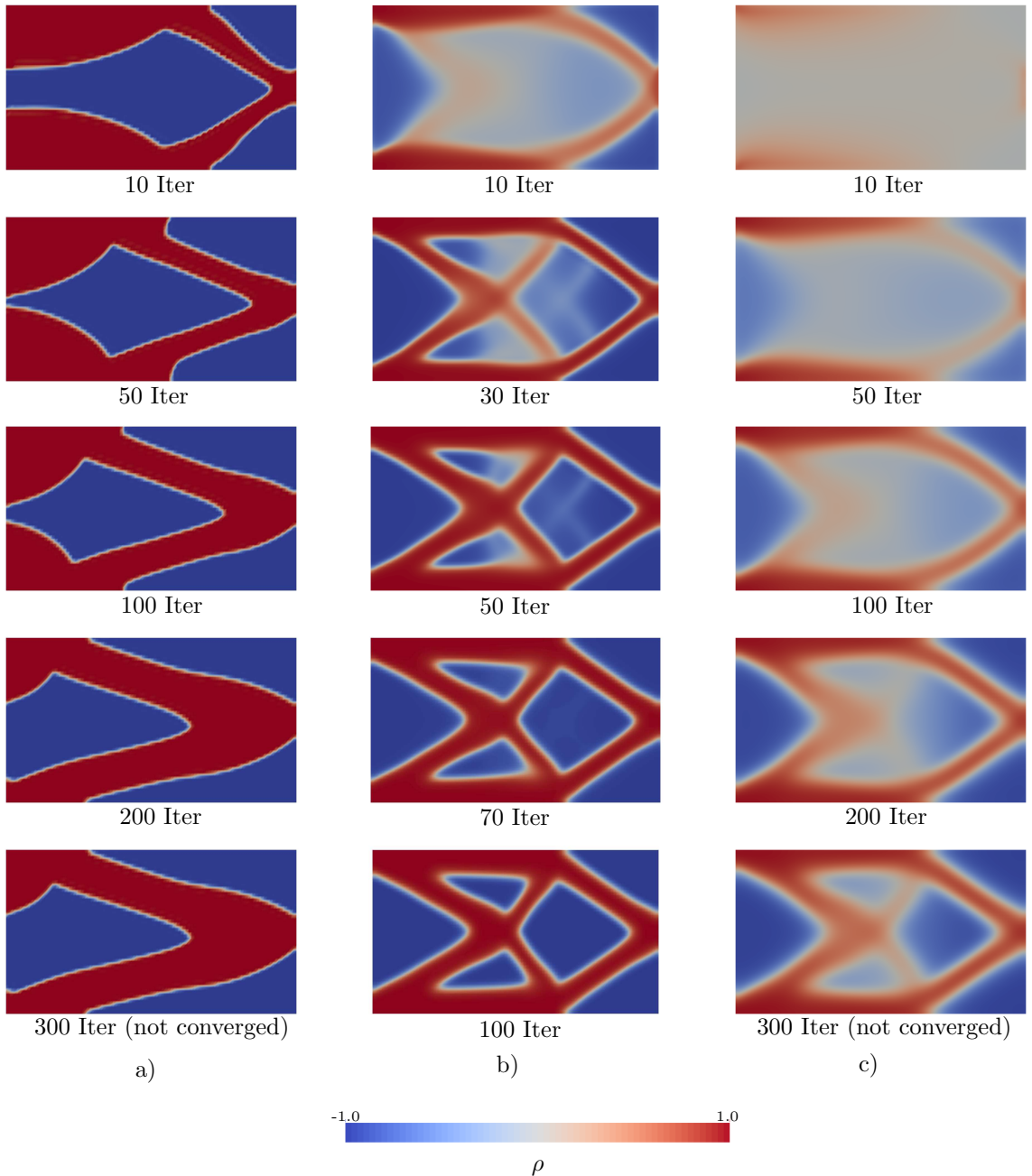


Figure 17: Comparison of different η_ξ (TK10), with unchanged other parameters and 0 initial state, a) $\eta_\xi = 0.0001$, b) $\eta_\xi = 0.001$, c) $\eta_\xi = 0.01$.

η is a factor multiplied to the Lagrangian composed of objective function and constraint

in (5.4) according to [70]. It balances the effects between the Lagrangian \mathcal{L} and other terms, e.g. interface, double well energy. A higher η will result in a clearer final state. The smaller it is, the more diffusion will be present in the evolution.

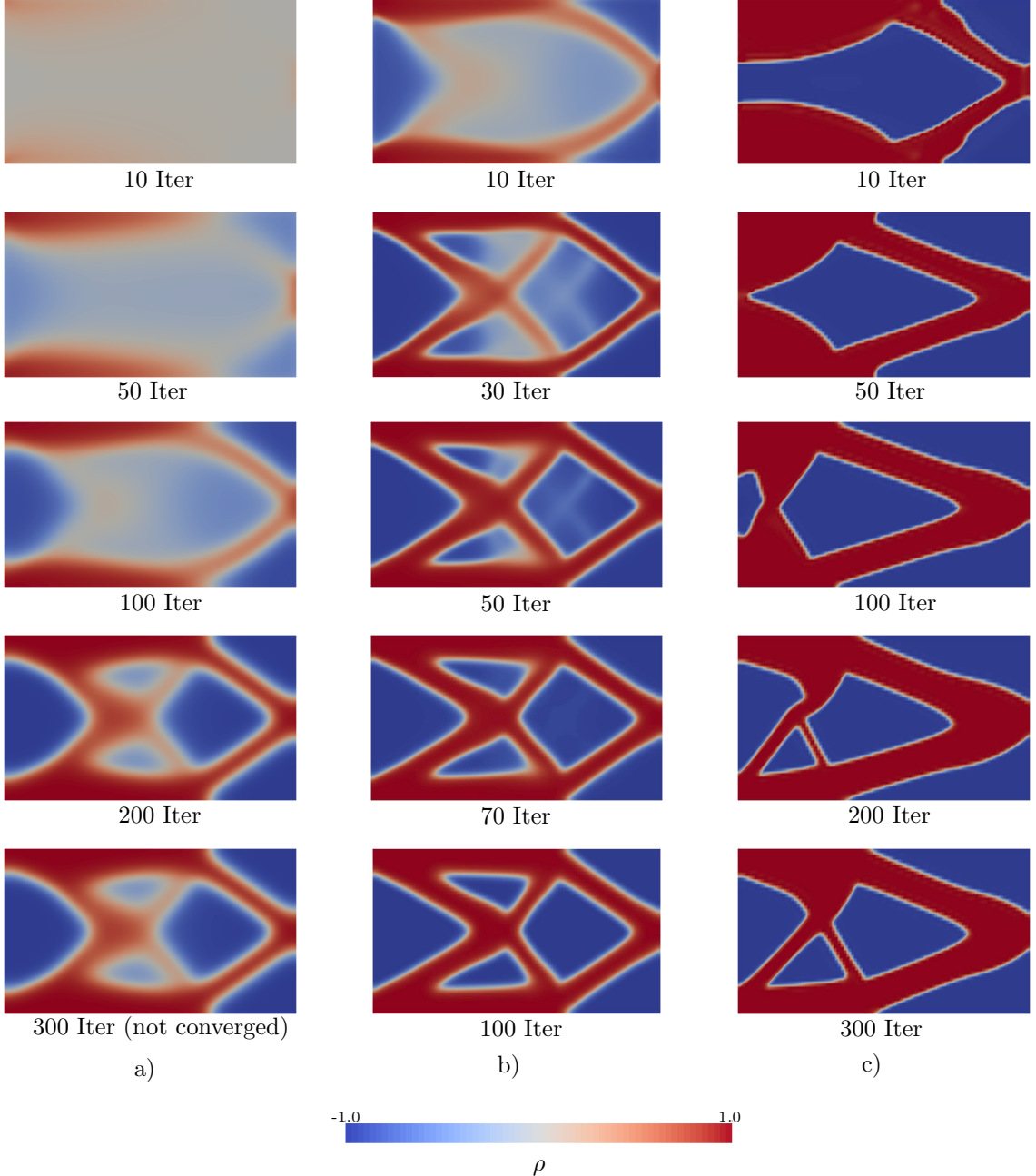


Figure 18: Comparison of different η (TK10), with unchanged other parameters and 0 initial state, a) $\eta = 1$, b) $\eta = 20$, c) $\eta = 200$.

The weight of objective function η_F in (4.7) is critical for optimization. c) in Figure 19 shows that high objective weight will blow up the design variable, since the homogeneous state with value 1 will achieve the minimum compliance. After 50 iterations holes are nucleated in the evolution in the c). The evolution in c) also reveals that too large weight also harms the complexity of the final pattern. The results of other two cases are rather identical.

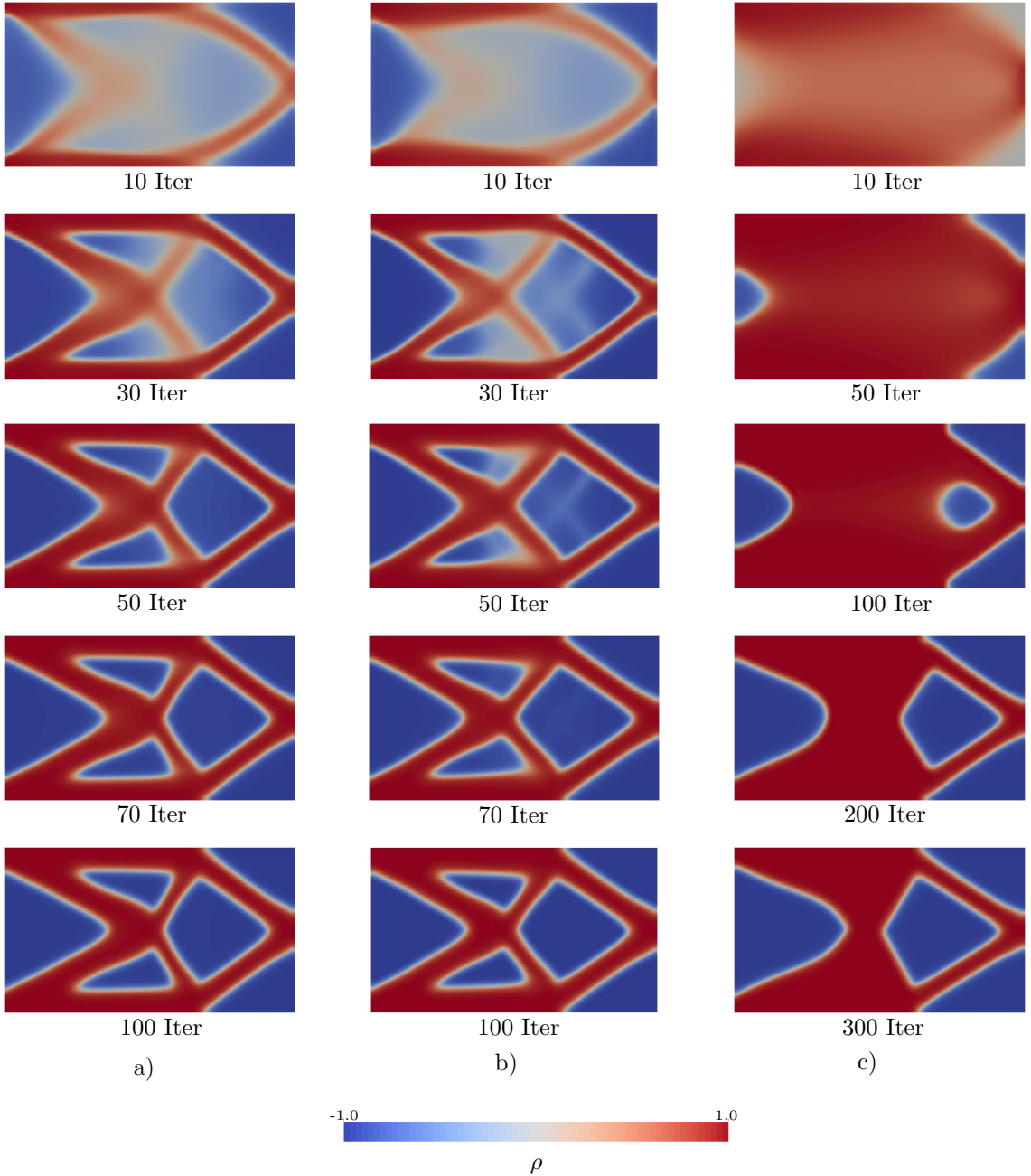


Figure 19: Comparison of different η_F (TK10), with unchanged other parameters and 0 initial state, a) $\eta_F = 1 \times 10^3$ (Lagrange multiplier and penalty is adjusted to stabilize the simulation), b) $\eta_F = 1 \times 10^5$, c) $\eta_F = 1 \times 10^7$.

Figure 20 shows that the penalty μ has the least effect on the evolution. This is consistent with the theoretical results for the augmented Lagrangian method [46].

Comparison of parameters in WL13 (incremental variational formulation) gives some interesting insights on the problem. In Figure 21, smaller interface energy weight leads to sharper interface. We hence conjecture that when this parameter $\eta_\xi \rightarrow 0$, a clear separation of material and void can be obtained. This is coherent with the convergence analysis in the paper [15]. Figure 22 demonstrates the influence of η_F . Similar with TK10, the results of WL13 also shows that the objective function weight has effects

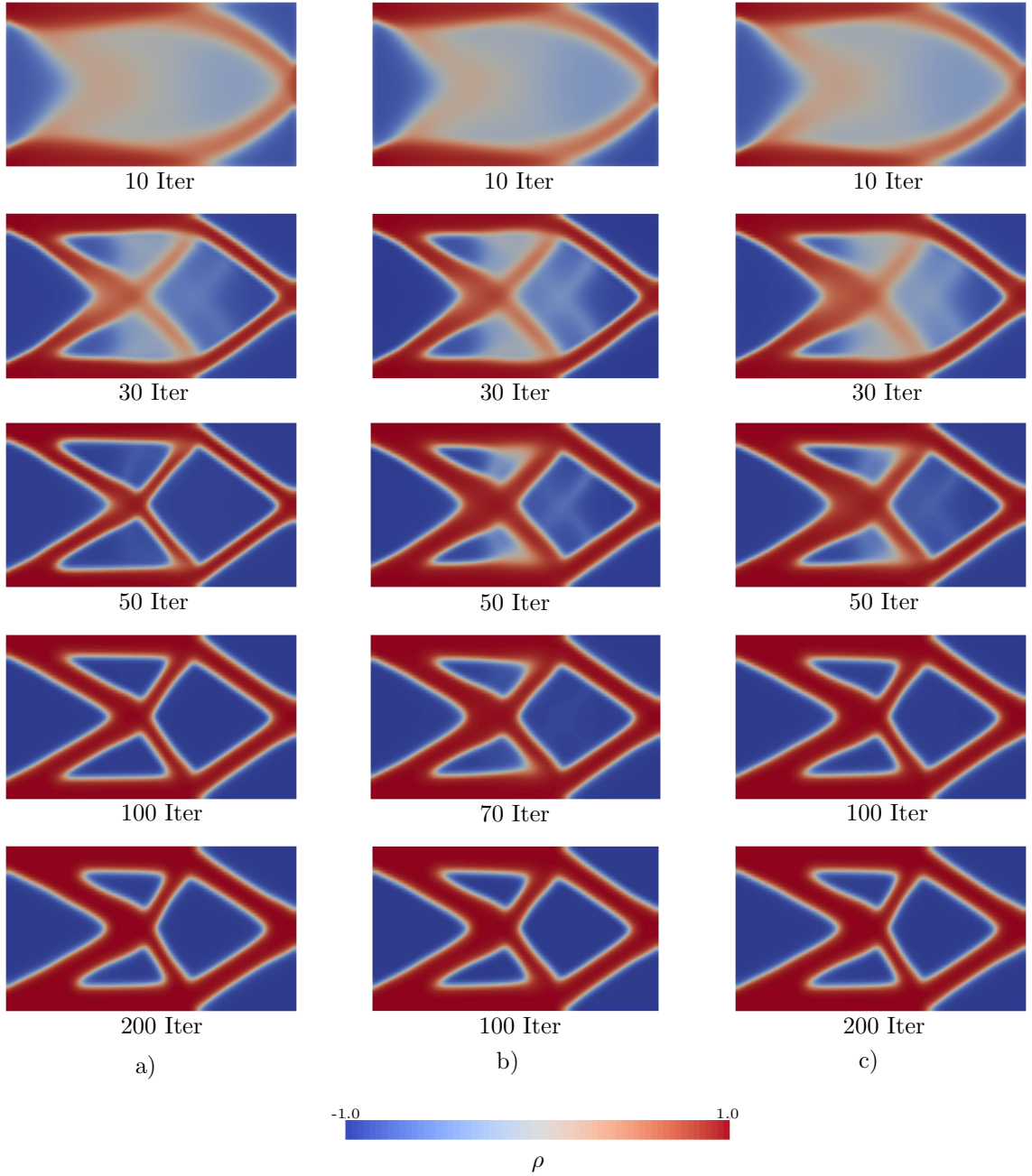


Figure 20: Comparison of different penalty parameters μ in augmented Lagrangian method (TK10), with unchanged other parameters and 0 initial state, a) $\mu = 1$, b) $\mu = 10$, c) $\mu = 100$.

on the complexity of final pattern. If too small weight is chosen, a spurious result is generated, while larger weight gives more detail. The final pattern of the larger weight case reminds us the pattern in [80], where different complexity is attained by tuning the diffusion coefficient. In the last comparison of the incremental variational formulation we see that the penalty parameter in augmented Lagrangian method also influences the end result. This is not what we expected. The reason may lie in that we approximate the second derivative of penalty term with a mass matrix.

Summary of Parameters

In this section we give a summary about the parameter choice. This is best presented

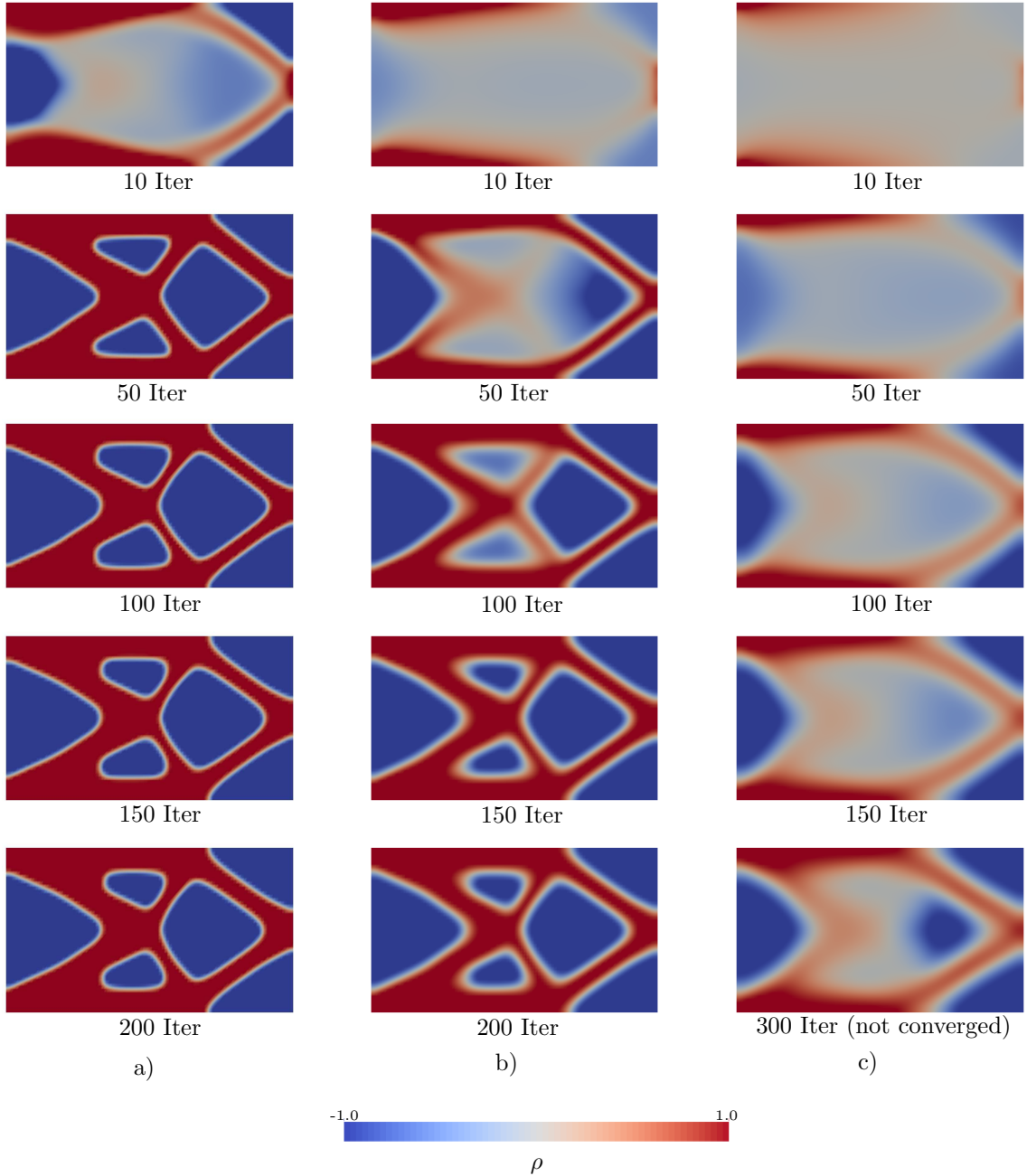


Figure 21: Comparison of different η_ξ (WL13), with unchanged other parameters and 0 initial state, a) $\eta_\xi = 0.02$, b) $\eta_\xi = 0.05$, c) $\eta_\xi = 0.2$.

in the following Table 12 and Table 13. We use ‘+’ to represent a positive correlation, ‘-’ a negative correlation, ‘0’ for no obvious correlation, and ∗ for not given. For example, ‘0, -, +’ for η_F means that η_F has no relation with the interface width, the larger the parameter, the less complex the final pattern is, and the larger the parameter, the more iteration number it needs to find the optimum state. It is important to note that this summary is obtained from the numerical experience. More attention needs to be paid to the theoretical aspect.

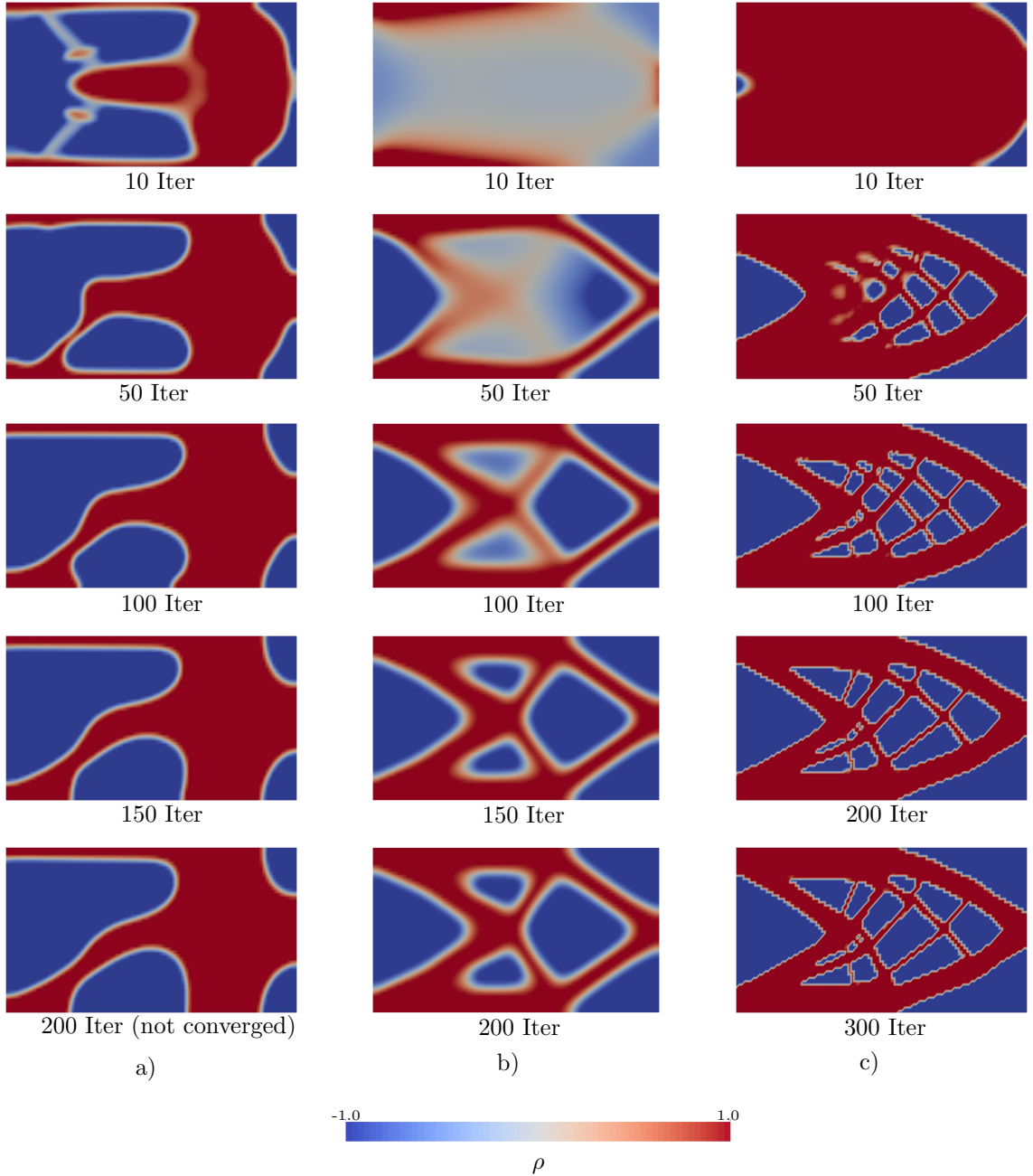


Figure 22: Comparison of different η_F (WL13), with unchanged other parameters and 0 initial state, a) $\eta_F = 1 \times 10^3$, b) $\eta_F = 1 \times 10^5$, c) $\eta_F = 1 \times 10^7$.

5.1.2. 3D Cantilever Beam

In this part we solve the optimization problem for 3D cantilever beam. The layout of the problem is presented in Figure 24. The problem formulation is the same as (5.1). Material parameters are also the same, while the parameters for optimization are different from the previous one and are given in Table 14.

And the optimization results are plotted in Figure 25. Both results are reasonable and have good match with those in [70]. However, the evolution animations of both fine and coarse mesh show some oscillation and the visualization is zigzagged by discrete elements. One remedy for the zigzagged results is to have a finer mesh or apply post processing

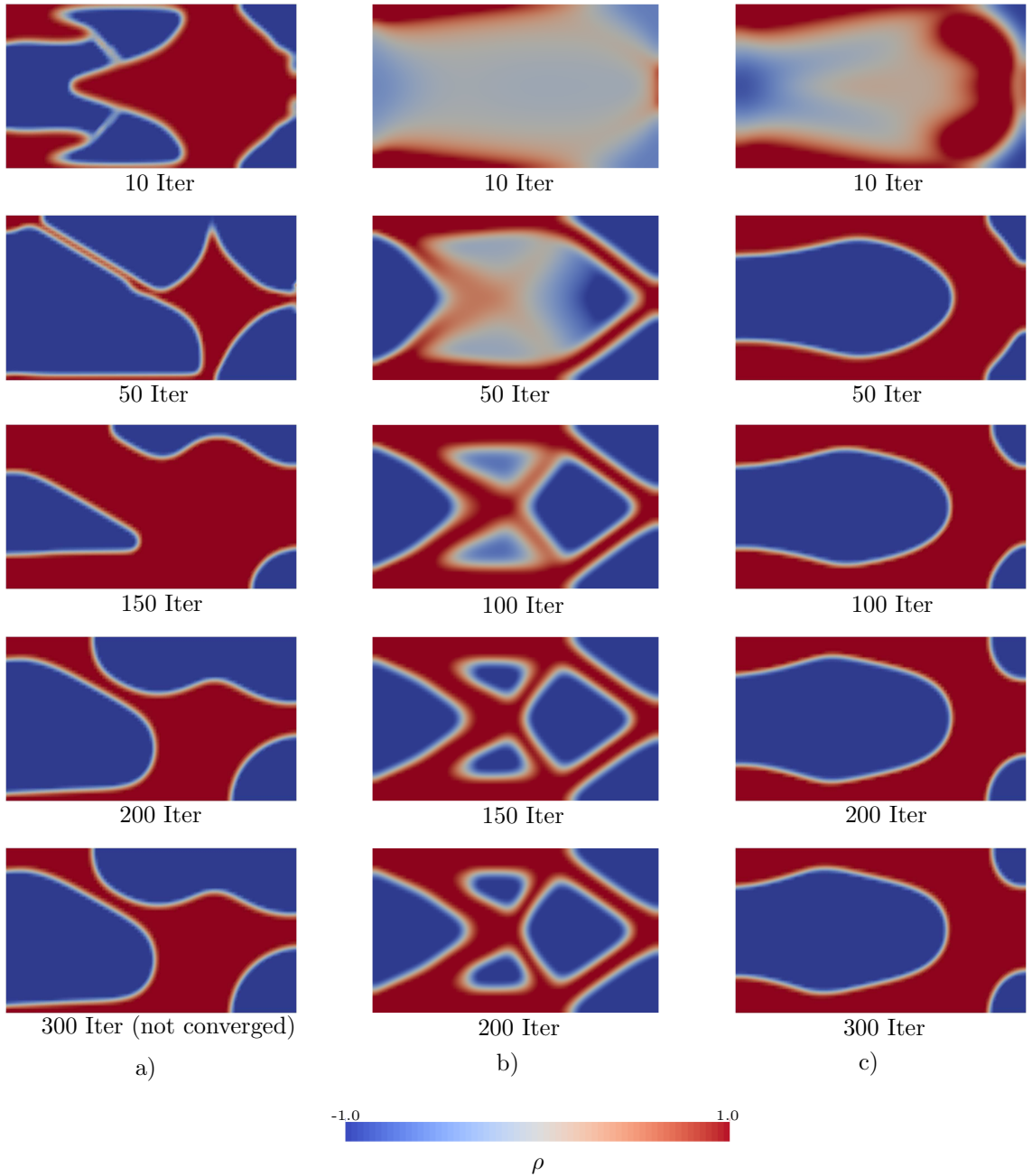


Figure 23: Comparison of different penalty parameters μ in augmented Lagrangian method (WL13) with unchanged other parameters and 0 initial state, a) $\mu = 1$, b) $\mu = 10$, c) $\mu = 100$.

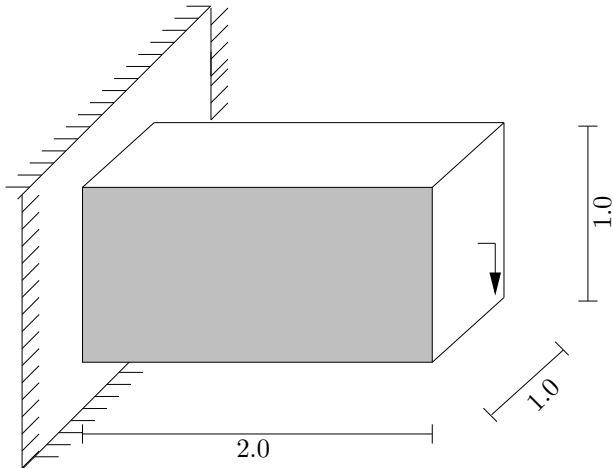
on the result. The speed of 3D optimization falls down tremendously. Hence for 3D optimization efficiency of the algorithm needs to be improved.

Table 12: Parameters in TK10 (reaction diffusion equation).

	Clear interface	Complexity	Iteration number
η_ξ	-	+	★
η	+	★	★
η_F	0	-	+
μ	0	0	0

Table 13: Parameters in WL13 (incremental variational formulation).

	Clear interface	Complexity	Iteration number
η_ξ	-	★	+
η_F	★	+	★
μ	0	-	★

**Figure 24:** 3D cantilever problem layout.**Table 14:** Optimization parameters for 3D cantilever.

Coarse mesh	Fine mesh
WL13	TK10
direct solver	iterative solver
$\eta_\xi = 0.1, \eta_F = 1 \times 10^6$	$\eta_\xi = 0.001, \eta_F = 1 \times 10^6$ $\eta = 40$
$\Delta t = 0.0125$	$\Delta t = 5 \times 10^{-5}$
$\lambda = -4, \mu = 1$	$\lambda = -4, \mu = 0.2$

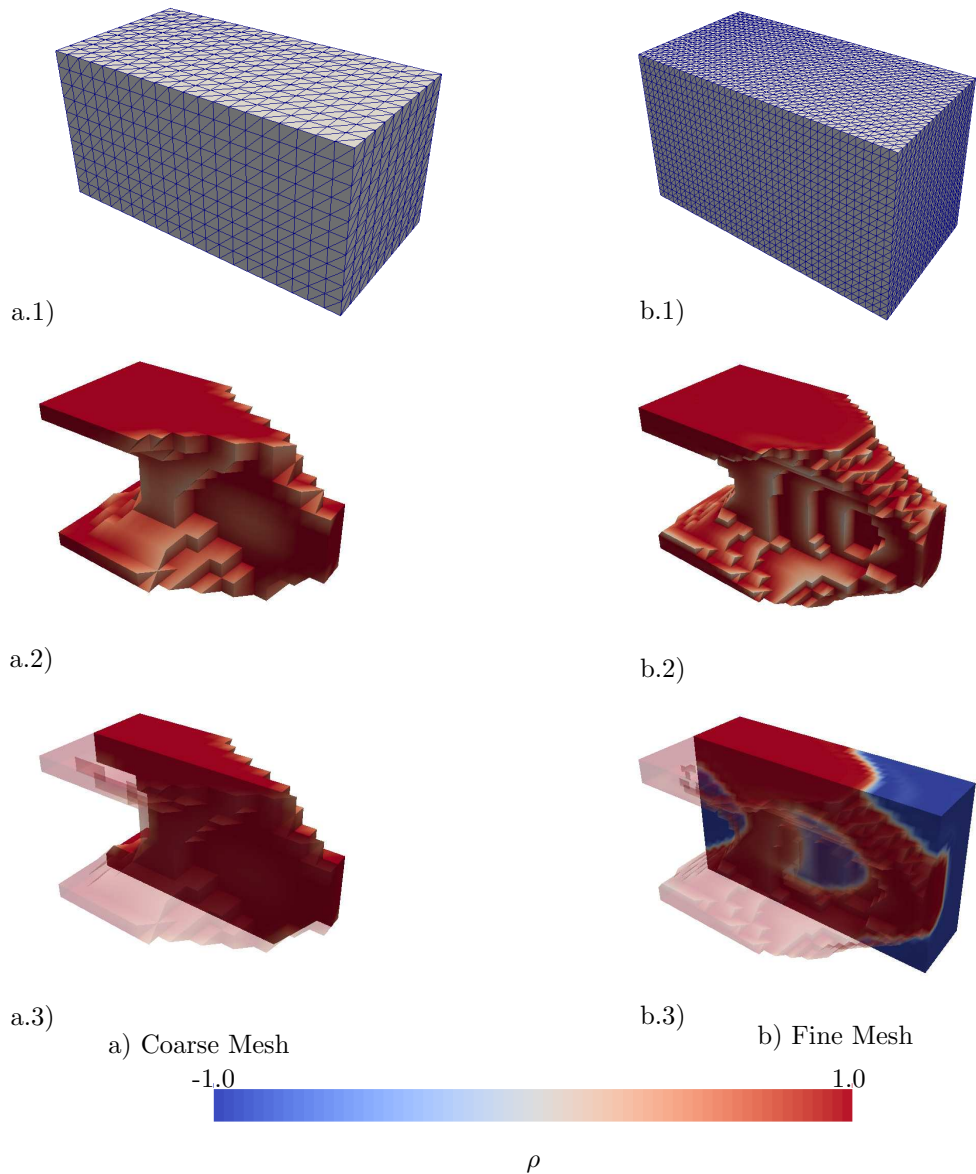


Figure 25: 3D cantilever beam, a) coarse mesh (WL13), 400th iteration, b) fine mesh iterative solver (TK10), 64th iteration.

5.2. Thermomechanical Problem

We consider a thermomechanical problem. This example is given in many publications, such as [71], [54], [81], and [79]. Among them the second one [54] is the earliest work on this problem which also includes homogenization technique. The last paper [54] employs the level set approach to tackle the problem. The first publication [71] is a master thesis on this topic including an extensive review and some engineering examples.

The layout of this basic problem is rendered in Figure 26, where a two side clamped beam is considered. The material model is written as below,

$$\boldsymbol{\varepsilon} = \frac{1}{E} [(1 + \nu) \boldsymbol{\sigma} - \nu \operatorname{tr}(\boldsymbol{\sigma}) \mathbf{I}] + \alpha \Delta T \mathbf{I}. \quad (5.6)$$

A simple thermal induced stress is added. This thermal stress depends on the change of temperature ΔT . The material properties are set as follows $E = 1$, $\nu = 0.3$, $\alpha = 5 \times 10^{-4}$. A crossed triangular structured mesh is generated. We start from the homogeneous pattern with value 0 (an intermediate state, $|\rho| \leq 1$) and optimize the topology under different temperature difference. Besides the current target is still the minimum compliance (5.1).

We employ the incremental variational formulation, and the selected parameters are $\eta_\xi = 0.05$, $\eta_F = 1 \times 10^3$, except that for $\Delta T = 100$ we have $\eta_F = 1 \times 10^4$. The time step and Lagrange multiplier are set $\Delta t = 6.25 \times 10^{-4}$, $\lambda = -4$, $\mu = 10$ respectively.

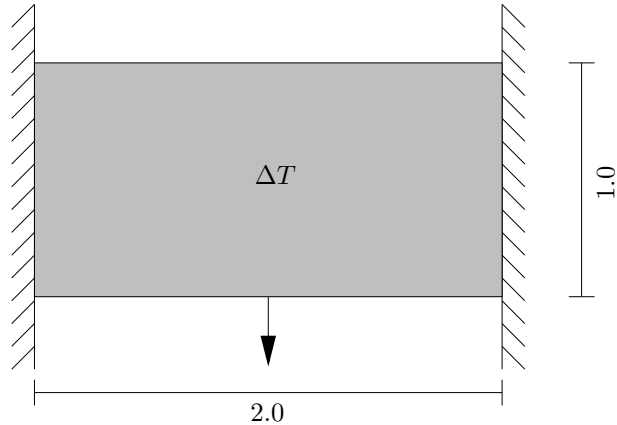


Figure 26: Thermomechanical problem layout.

The results are shown in Figure 27. And these results are consistent with the results given in [54]. In the process of evolution, we also observe the oscillation of states. This could be fixed by tuning a weaker penalty μ or a smaller time step.

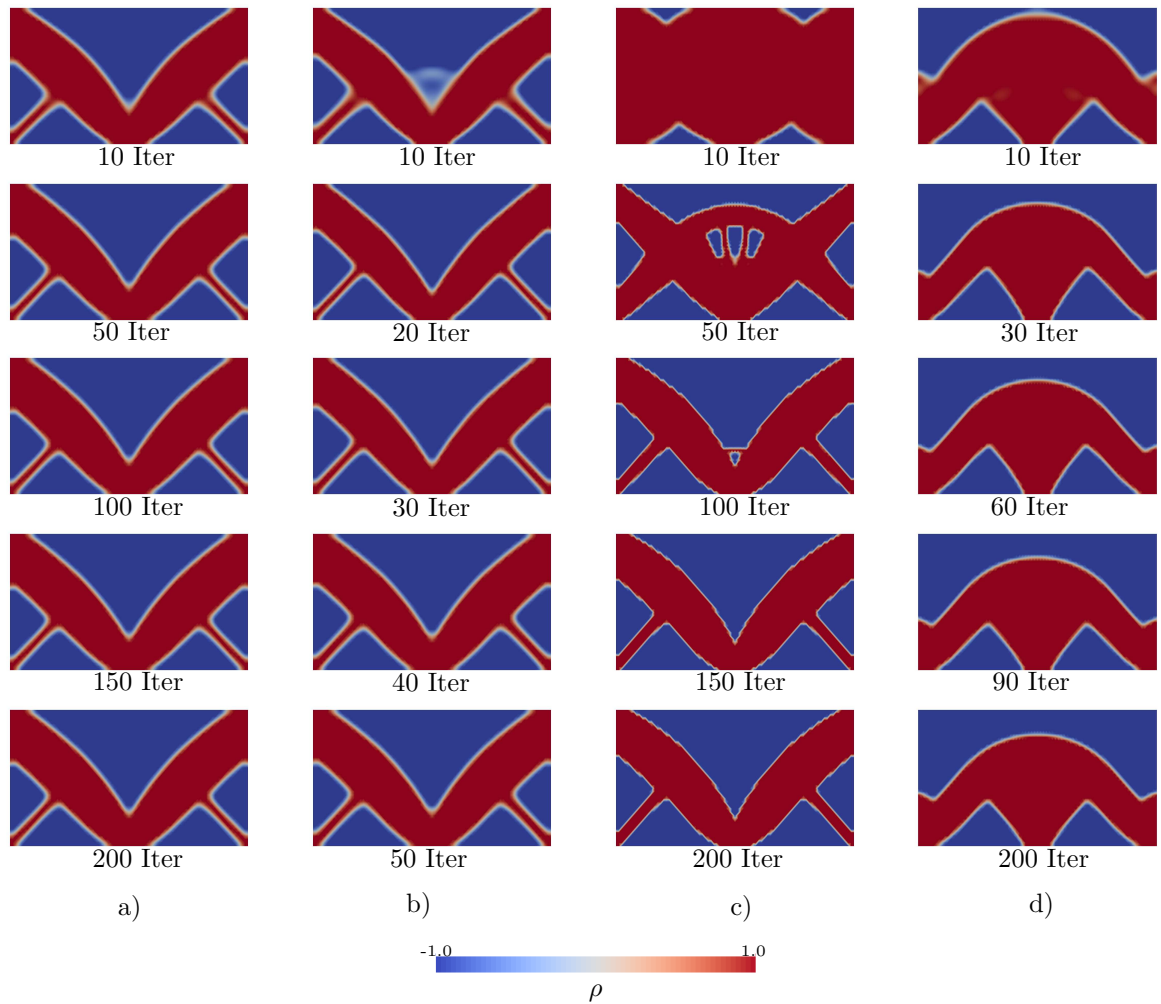


Figure 27: Comparison of different ΔT (WL13), a) $\Delta T = 0$, b) $\Delta T = 50$, c) $\Delta T = 100$, d) $\Delta T = 200$.

5.3. Coupled Electro-mechanical Unit Cell Optimization

At last we present a coupled-field unit cell example. The sketch of this problem is given in Figure 28 showing a unit square with fixed corners and two pairs of periodic boundary conditions. We consider a two-material topology optimization problem.

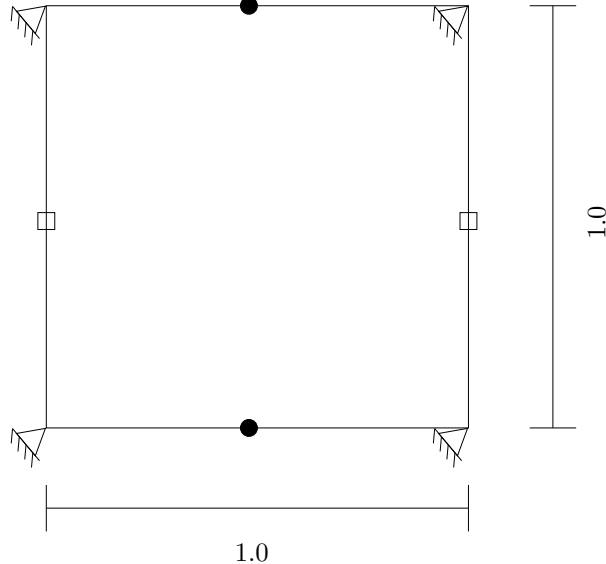


Figure 28: Unit cell optimization problem layout, with 4 fixed corners and periodic boundary condition for pairing edges.

We use a Neo-Hookean type electroactive polymer material, as in [36],

$$\psi(\mathbf{C}, \mathbf{E}) = \frac{1}{2}\mu(\text{tr}[\mathbf{C}] - 3) + \frac{\lambda}{4}(J^2 - 1) - \left(\frac{\lambda}{2} + \mu\right)\ln J - \frac{1}{2}\epsilon_0\left(1 + \frac{\chi}{J}\right)J[\mathbf{C}^{-1} : (\mathbf{E} \otimes \mathbf{E})], \quad (5.7)$$

where λ and μ are Lamé constants and χ is the electric susceptibility. ϵ_0 is the electric permittivity in vacuum and taken as 8.85×10^{-12} . The variable in this material model is \mathbf{C} (right Cauchy-Green tensor), J defined as $\det \mathbf{F}$ (\mathbf{F} is the deformation gradient tensor), and \mathbf{E} the electric field. The two materials in our example are a stiff material with high electric susceptibility representing metal phase, and a soft material phase with relative low electric susceptibility such as rubber. We use a simple material interpolation (5.8)

Table 15: Material parameters of unit cell.

	Young's Modulus	Poisson Ratio	Electric Susceptibility
Soft material phase	1	0.3	7
Metal phase	1000	0.4	700

with a scaling function. For other multi material interpolation reader can refer to [12].

$$\begin{aligned} E &= g(\rho)E_{\text{sof}} + (1 - g(\rho))E_{\text{met}}, \\ \nu &= g(\rho)\nu_{\text{sof}} + (1 - g(\rho))\nu_{\text{met}}, \\ \chi &= g(\rho)\chi_{\text{sof}} + (1 - g(\rho))\chi_{\text{met}}. \end{aligned} \quad (5.8)$$

“sof” in the subscript stands for soft rubber-like material and “met” for metal-like material. $g(\rho)$ is given in (5.2).

The formulation of the PDE constraint follows the one in [57]. The details can be viewed in this paper. We use homogenization technique [23]. We denote $\bar{(\cdot)}$ as the averaged macro field variable and $\tilde{(\cdot)}$ as the micro field fluctuation. The macro field variables are taken as $\bar{\mathbf{F}}$, $\bar{\mathbf{E}}$. Boundary conditions for this problem is a periodic one, meaning the field variable $\tilde{\mathbf{u}}$, $\tilde{\phi}$ match for the opposite edges. In order to prevent the rigid body displacement, we prescribe the corners to be fixed. Linear triangular finite element is used for the analysis of both PDE constraint and evolution step. The mesh is a crossed structured mesh presented below and the element size is $1/30$, and in total $30 \times 30 \times 4 = 3600$ elements are in use. We input the following macro field variable.

$$\bar{\mathbf{F}} = \begin{bmatrix} 1 & 0 \\ 0 & 1 \end{bmatrix}, \bar{\mathbf{E}} = \begin{bmatrix} 0 \\ 0.2 \end{bmatrix}$$

Our goal in this type of optimization problem is to achieve a microstructure design as in [69]. We considered a simplified topology optimization problem. Under a specific input of the macro electric field, we maximize the traction on the upper bound of this representative element. The physical meaning is that, we want to achieve the largest mechanical response under the macro averaged electric field. The complete optimization problem is stated as follows,

$$\begin{aligned} \min_{\rho} \quad & F(\mathbf{u}, \rho) = - \int_{\partial\Omega_u} (\mathbf{P}\mathbf{n}) \cdot \mathbf{n} \, dS \\ \text{subject to} \quad & C_{\text{vol}}(\rho) = \int_D \rho \, dV - V_0 \leq 0, \\ & G(\mathbf{u}, \rho) = 0 \text{ (Nonlinear PDE),} \\ & -1 \leq \rho \leq 1. \end{aligned} \tag{5.9}$$

We write the objective function with respect to the first Piola-Kirchhoff stress tensor \mathbf{P} . In the expression \mathbf{n} is the normal vector of the surface, so $(\mathbf{P}\mathbf{n}) \cdot \mathbf{n}$ is the normal component of surface traction. With the integration we obtain the averaged traction over the upper bound. The current PDE constraint is a nonlinear PDE with macro field input under periodic boundary constraint. We refer to [57] for details. We denote $\partial\Omega_u$ as the upper bound of the unit cell.

Various initial patterns are solved using the incremental variational formulation. Optimization parameters are given in (5.10). The volume of metal phase is constrained to be 50 % of the design domain.

$$\eta_\xi = 0.05, \quad \eta_F = 1, \quad \Delta t = 0.0022, \quad \lambda = -1, \quad \mu = 4. \tag{5.10}$$

Note that we have used a time step as $0.2\Delta t_{\text{cfl}}$ and t_{cfl} is defined in (4.27).

If we fix the volume and let SNES handle the Lagrange multiplier internally, we can achieve optimum state very fast. In contrary, there is more oscillation in the incremental variational formulation. This oscillation is caused by the augmented Lagrangian algorithm, where each iteration the Lagrange multiplier is approximated using the penalty parameter and the current constraint value. If the right Lagrange multiplier is supplied initially, the design variable can converge to the optimum state very fast without or with just minor oscillation.

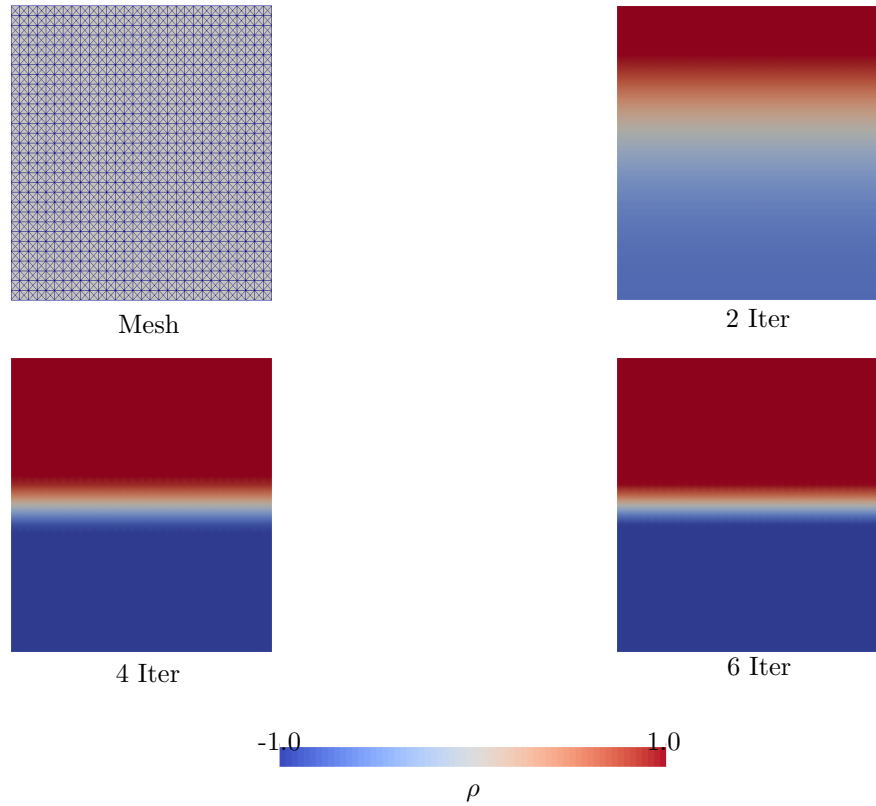


Figure 29: Unit cell optimization (WL13), fixed volume optimization, Lagrange multiplier is accounted internally in SNES, two materials, 0.5 volume fraction of one material is specified.

For different initial patterns, we have the same final result. The optimization process shows that in this problem, the design variable is firstly diffused to all -1. Then an identical optimization process is carried out till the optimum is reached.

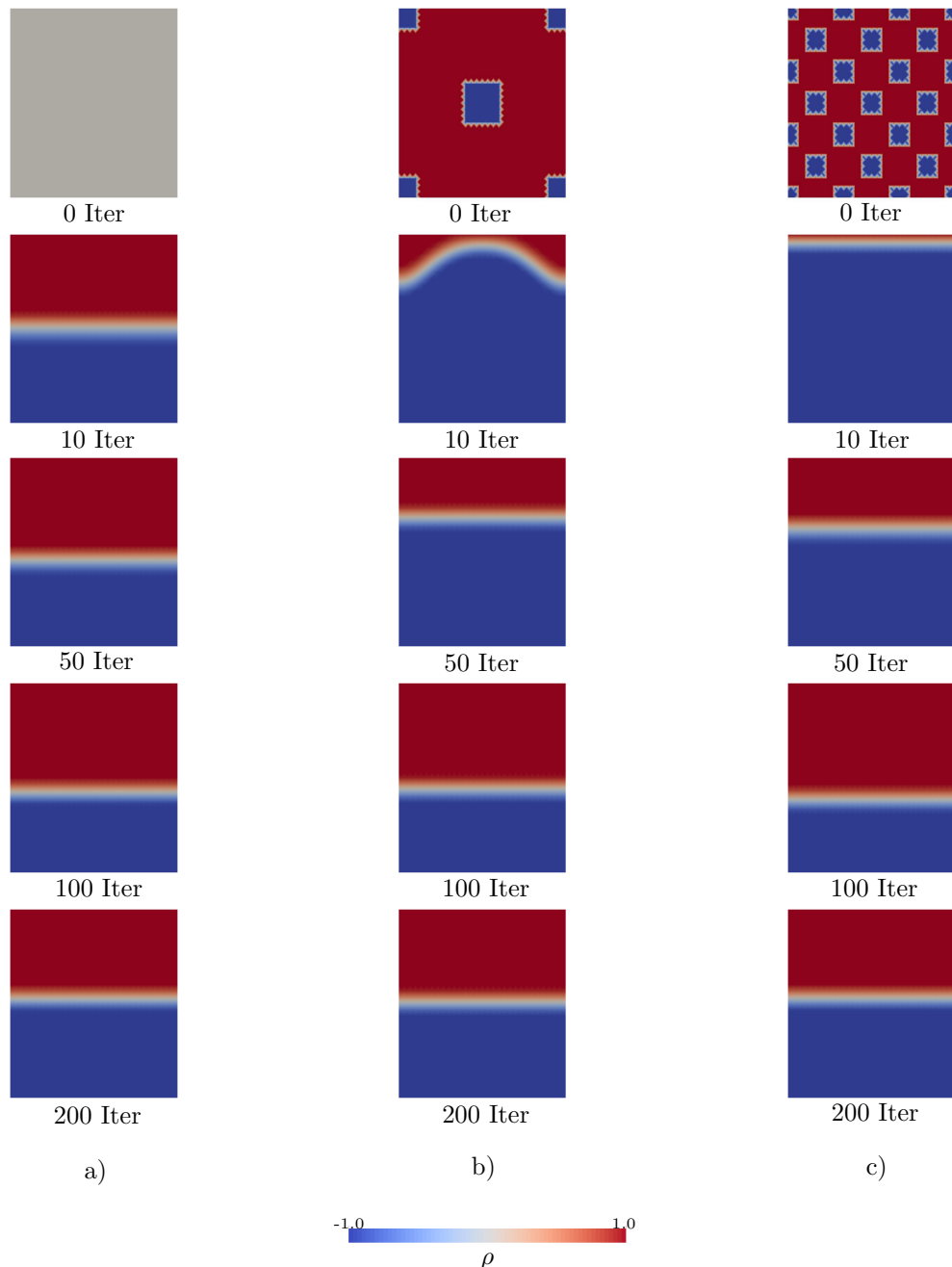


Figure 30: Comparison of different initial states for unit cell optimization (WL13), a) homogeneous initial state with 0, b) initial state with a central hole, d) initial state with many holes.

6. Conclusion

In this thesis classical SIMP method and its techniques were reviewed at first, then we briefly discussed about the level set method and moved on to the phase field approach. Two different formulations of the phase field approach are analyzed, namely Takezawa's approach [70], and Wallin's approach [73]. Based on them two generalized formulations (4.7) and (4.16) are given. Furthermore the augmented Lagrangian method and Algorithm 1 are adjusted and applied to these formulations. With two topology optimization algorithms in Algorithm 2 and Algorithm ??, we first verified the methods with the basic cantilever compliance problem, then discussed about the parameter choice of both formulations extensively. A 3D cantilever problem, a thermoelastic problem, and a coupled-field unit cell optimization problem have also been considered.

We show that the phase field approach for topology optimization is a valid approach and can be further applied to more complex problems. Problems such as checkerboard patterns and reinitialization occurring in the standard SIMP and the level set method are alleviated. We include a phase field energy consisting of double well potential and interface energy in the Lagrangian. These two parts of phase field energy play different roles in the optimization (discussed in 2.2.3) – the double well potential can be regarded as a penalty for the intermediate state, the interface energy term is a global constraint, which will regularize the optimization problem. Moreover an incremental variational formulation inspired by [40] is developed. Compared with the standard optimization formulation in the SIMP method, the incremental variational formulation can be deemed as a damped optimization problem (see in 4.2.2) and allows us to make stabler progress in the course of optimization. Besides, the augmented Lagrangian method is applicable in the context of topology optimization.

The weaknesses of the phase field approach can also be seen immediately. The primal one is too many parameters. It is not trivial to obtain an appropriate weight for each term in the formulation (4.7) and (4.16). Techniques should be invented to circumvent this problem. Another problem comes from the nature of augmented Lagrangian method. As can be seen in 5.1.1 and Figure 11 the result tends to oscillate when the Lagrange multiplier and the penalty is not wisely chosen. Hence a careful choice of Lagrange multiplier and penalty parameter to achieve faster and stabler convergence.

Many improvements can be made to the current approaches. The crucial one is scaling. If a good scaling can be found, it will guide our choice of weight of each term in (4.7) and (4.16) and finally resolve the problem of parameter setting. As revealed in the previous chapter of numerical results, the weight parameters relates strongly with the complexity of the end design pattern. Hence continuation schemes can be developed. A feasible idea is to first make the problem well-posed by choosing proper parameters, then adapt the parameters so that sharp interface or hole nucleation is achieved. [68] gives some reflection on continuation method in its later part, and recent work about the continuation method is given in [55]. The theoretical support of the continuation method is from [15], where the sharp interface limit of phase field approach is proven. Another possibility of improvement is to develop more precise numerical schemes. We can include the second order sensitivity analysis in our optimization algorithm, although it is still a challenge to compute it correctly and efficiently. At least some approximated second order sensitivity information can be obtained by Hessian approximation using BFGS. When it comes to large scale problems, one is always cautious about efficiency. This urges us to

include modern numerical techniques in topology optimization such as homogenization with respect to a unit cell, model order reduction and parallelization.

A. Detailed Comparison of TK10 and WL13

Table 16: Comparison of f_{src} .

TK10	$f_{\text{src}} = \frac{\partial}{\partial \rho} (\eta_\psi \psi + G(x)g(\rho))$
WL13	$f_{\text{src}} = \frac{\partial}{\partial \rho} (\eta_\psi \psi + \eta_F F - \lambda c_{\text{vol}})$

In the subsection 4.2.3, we have the comparison summarized in the above tables. The definition of $G(x)$ and $g(\rho)$ are given below,

$$G(x) = \eta \frac{\mathcal{L}'(\rho_k)}{\|\mathcal{L}'(\rho_k)\|}, \quad g(\rho) = 6\rho^5 - 20\rho^3 + 30\rho, \quad (\text{A.1})$$

with the Lagrangian \mathcal{L} defined as $\mathcal{L} = F - \lambda C_{\text{vol}}$. Hence the main difference lies $G(x)g(\rho)$ in TK10 and $\eta_F F - \lambda c_{\text{vol}}$ in WL13. We have for TK10,

$$\frac{\partial}{\partial \rho} (G(x)g(\rho)) = \eta \frac{\mathcal{L}'(\rho_k)}{\|\mathcal{L}'(\rho_k)\|} \frac{\partial g(\rho)}{\partial \rho} = \eta \frac{\partial_\rho g(\rho)}{\|\mathcal{L}'(\rho_k)\|} \left(\frac{\partial F}{\partial \rho} \Big|_{\rho_k} - \lambda \frac{\partial c_{\text{vol}}}{\partial \rho} \Big|_{\rho_k} \right). \quad (\text{A.2})$$

Meanwhile we obtain the derivative of $\eta_F F - \lambda c_{\text{vol}}$ in WL13,

$$\frac{\partial}{\partial \rho} (\eta_F F - \lambda c_{\text{vol}}) = \eta_F \frac{\partial F}{\partial \rho} \Big|_{\rho_k} - \lambda \frac{\partial c_{\text{vol}}}{\partial \rho} \Big|_{\rho_k}. \quad (\text{A.3})$$

The partial derivative of objective F in the above two derivations represent the sensitivity of F in the sense of local form as in the appendix of [70]. Both of them are evaluated at the previous design variable ρ_k meaning a linearization of the objective F , which is discussed in the section 4.3. The difference in the weight of two derivatives can be summarized in the following table. We realize that the weights in TK10 have a part depending on the previous design variable ρ_k . It determines the effect of the gradient of objective function and constraint respectively.

Table 17: Comparison of weights.

	$\frac{\partial F}{\partial \rho}$	$-\frac{\partial c_{\text{vol}}}{\partial \rho}$
TK10	$\eta \frac{\partial_\rho g(\rho)}{\ \mathcal{L}'(\rho_k)\ }$	$\eta \frac{\partial_\rho g(\rho)}{\ \mathcal{L}'(\rho_k)\ } \lambda$
WL13	η_F	λ

References

- [1] ALLAIRE, G.; DAPOGNY, C.; FREY, P. [2013]: *A mesh evolution algorithm based on the level set method for geometry and topology optimization*. Structural and Multidisciplinary Optimization, 48(4): 711–715.
- [2] ALLAIRE, G.; JOUVE, F.; TOADER, A.-M. [2002]: *A level-set method for shape optimization*. Comptes Rendus Mathematique, 334(12): 1125–1130.
- [3] ALLAIRE, G.; JOUVE, F.; TOADER, A.-M. [2004]: *Structural optimization using sensitivity analysis and a level-set method*. Journal of Computational Physics, 194(1): 363–393.
- [4] ALLAIRE, G.; PANTZ, O. [2006]: *Structural optimization with FreeFem++*. Structural and Multidisciplinary Optimization, 32(3): 173–181.
- [5] ALTAIR ENGINEERING INC: *OptiStruct 12.0 User's Guide*.
- [6] ARORA, J.S.; WANG, Q. [2005]: *Review of formulations for structural and mechanical system optimization*. Structural and Multidisciplinary Optimization, 30(4): 251–272.
- [7] BALAY, S.; ABHYANKAR, S.; ADAMS, M.; BROWN, J.; BRUNE, P.; BUSCHELMAN, K.; DALCIN, L.; EIJKHOUT, V.; GROPP, W.; KAUSHIK, D.; KNEPLEY, M.; MCINNES, L.; RUPP, K.; SMITH, B.; ZAMPINI, S.; ZHANG, H. [2016]: *PETSc Users Manual*. Technical Report ANL-95/11 - Revision 3.7, Argonne National Laboratory.
- [8] BAÑAS, L.; NÜRNBERG, R. [2008]: *Adaptive finite element methods for Cahn-Hilliard equations*. Journal of Computational and Applied Mathematics, 218(1): 2–11.
- [9] BELYTSCHKO, T.; XIAO, S.; PARIMI, C. [2003]: *Topology optimization with implicit functions and regularization*. International Journal for Numerical Methods in Engineering, 57(8): 1177–1196.
- [10] BENDSØE, M.P. [1989]: *Optimal shape design as a material distribution problem*. Structural optimization, 1(4): 193–202.
- [11] BENDSØE, M.P.; KIKUCHI, N. [1988]: *Generating Optimal Topologies in Structural Design Using a Homogenization Method*. Comput. Methods Appl. Mech. Eng., 71(2): 197–224.
- [12] BENDSØE, M.P.; SIGMUND, O. [1999]: *Material interpolation schemes in topology optimization*. Archive of Applied Mechanics, 69(9-10): 635–654.
- [13] BENDSØE, M.P.; SIGMUND, O. [2004]: *Topology Optimization*. Springer Berlin Heidelberg, Berlin, Heidelberg.
- [14] BLANK, L.; FARSHBAF-SHAKER, M.; GARCKE, H.; RUPPRECHT, C.; STYLES, V. [2013]: *Multi-material phase field approach to structural topology optimization*. arXiv:1312.2356 [math].
- [15] BLANK, L.; GARCKE, H.; HECHT, C.; RUPPRECHT, C. [2014]: *Sharp interface limit for a phase field model in structural optimization*. arXiv:1409.7586 [math].

- [16] BLANK, L.; GARCKE, H.; SARBU, L.; SRISUPATTARAWANIT, T.; STYLES, V.; VOIGT, A. [2012]: *Phase-field approaches to structural topology optimization*. In *Constrained Optimization and Optimal Control for Partial Differential Equations*, pp. 245–256. Springer.
- [17] BOETTINGER, W. J.; WARREN, J. A.; BECKERMAN, C.; KARMA, A. [2002]: *Phase-Field Simulation of Solidification*. Annual Review of Materials Research, 32(1): 163–194.
- [18] BORRVALL, T.; PETERSSON, J. [2001]: *Topology optimization using regularized intermediate density control*. Computer Methods in Applied Mechanics and Engineering, 190(37): 4911–4928.
- [19] BURGER, M.; STAINKO, R. [2006]: *Phase-Field Relaxation of Topology Optimization with Local Stress Constraints*. SIAM Journal on Control and Optimization, 45(4): 1447–1466.
- [20] CACUCI, D.G. [1981]: *Sensitivity theory for nonlinear systems. I. Nonlinear functional analysis approach*. Journal of Mathematical Physics, 22(12): 2794–2802.
- [21] CACUCI, D.G. [2016]: *Second-order adjoint sensitivity analysis methodology (2nd-asam) for large-scale nonlinear systems: I. Theory*. arXiv:1601.06609 [math].
- [22] CHEN, L.Q. [2002]: *Phase-Field Models for Microstructure Evolution*. Annual Review of Materials Research, 32(1): 113–140.
- [23] CIORANESCU, D.; DONATO, P. [2000]: *An Introduction to Homogenization*. Oxford University Press, Oxford ; New York, 1 edition Edition.
- [24] DIJK, N. P. VAN; MAUTE, K.; LANGELAAR, M.; KEULEN, F. v. [2013]: *Level-set methods for structural topology optimization: a review*. Structural and Multidisciplinary Optimization, 48(3): 437–472.
- [25] FRIED, E.; GURTIN, M. E. [1993]: *Continuum theory of thermally induced phase transitions based on an order parameter*. Physica D: Nonlinear Phenomena, 68(3): 326–343.
- [26] FUNKE, S. W.; FARRELL, P. E. [2013]: *A framework for automated PDE-constrained optimisation*. arXiv:1302.3894 [cs].
- [27] GAIN, A.L.; PAULINO, G. [2013]: *A critical comparative assessment of differential equation-driven methods for structural topology optimization*. Structural and Multidisciplinary Optimization, 48(4): 685–710.
- [28] GHABRAIE, K. [2014]: *The ESO method revisited*. Structural and Multidisciplinary Optimization, 51(6): 1211–1222.
- [29] GLOWINSKI, R.; TALLEC, P. [1989]: *Augmented Lagrangian and Operator-splitting Methods in Nonlinear Mechanics*. SIAM.
- [30] GURTIN, M.E. [1996]: *Generalized Ginzburg-Landau and Cahn-Hilliard equations based on a microforce balance*. Physica D: Nonlinear Phenomena, 92(3): 178–192.
- [31] GURTIN, M.E.; POLIGNONE, D.; VIÑALS, J. [1996]: *Two-phase binary fluids and immiscible fluids described by an order parameter*. Mathematical Models and Methods in Applied Sciences, 06(06): 815–831.
- [32] HAFTKA, R.T. [1985]: *Simultaneous analysis and design*. AIAA Journal, 23(7): 1099–1103.

- [33] HAFTKA, R.T.; KAMAT, M. [1989]: *Simultaneous nonlinear structural analysis and design*. Computational Mechanics, 4(6): 409–416.
- [34] HUANG, X.D.; XIE, Y. [2010]: *A further review of ESO type methods for topology optimization*. Structural and Multidisciplinary Optimization, 41(5): 671–683.
- [35] KATO, J.; YACHI, D.; TERADA, K.; KYOYA, T. [2013]: *Topology optimization of micro-structure for composites applying a decoupling multi-scale analysis*. Structural and Multidisciplinary Optimization, 49(4): 595–608.
- [36] KEIP, M.-A.; STEINMANN, P.; SCHRÖDER, J. [2014]: *Two-scale computational homogenization of electro-elasticity at finite strains*. Computer Methods in Applied Mechanics and Engineering, 278: 62–79.
- [37] KRUIJF, N. DE; ZHOU, S.; LI, Q.; MAI, Y.-W. [2007]: *Topological design of structures and composite materials with multiobjectives*. International Journal of Solids and Structures, 44(22): 7092–7109.
- [38] LIU, K.; TOVAR, A. [2014]: *An efficient 3D topology optimization code written in Matlab*. Structural and Multidisciplinary Optimization, 50(6): 1175–1196.
- [39] LOGG, A.; WELLS, G. N. [2010]: *DOLFIN: Automated finite element computing*. ACM Transactions on Mathematical Software (TOMS), 37(2): 20.
- [40] MIEHE, C.; ETHIRAJ, G. [2012]: *A geometrically consistent incremental variational formulation for phase field models in micromagnetics*. Computer Methods in Applied Mechanics and Engineering, 245: 331–347.
- [41] MIEHE, C.; WELSCHINGER, F.; HOFACKER, M. [2010]: *Thermodynamically consistent phase-field models of fracture: Variational principles and multi-field FE implementations*. International Journal for Numerical Methods in Engineering, 83(10): 1273–1311.
- [42] MUNRO, D.; GROENWOLD, A. A. [2016]: *On sequential approximate simultaneous analysis and design in classical topology optimization*. International Journal for Numerical Methods in Engineering, pp. n/a–n/a.
- [43] NAKSHATRALA, P.B.; TORTORELLI, D. [2016]: *Nonlinear structural design using multiscale topology optimization. Part II: Transient formulation*. Computer Methods in Applied Mechanics and Engineering, 304: 605–618.
- [44] NAKSHATRALA, P.B.; TORTORELLI, D.; NAKSHATRALA, K. [2013]: *Nonlinear structural design using multiscale topology optimization. Part I: Static formulation*. Computer Methods in Applied Mechanics and Engineering, 261: 167–176.
- [45] NANTHAKUMAR, S. S.; LAHMER, T.; ZHUANG, X.; PARK, H. S.; RABCZUK, T. [2016]: *Topology optimization of piezoelectric nanostructures*. Journal of the Mechanics and Physics of Solids, 94: 316–335.
- [46] NOCEDAL, J.; WRIGHT, S. [2006]: *Numerical Optimization*. Springer Science & Business Media.
- [47] NORATO, J.A.; BENDSØE, M.; HABER, R.; TORTORELLI, D. [2007]: *A topological derivative method for topology optimization*. Structural and Multidisciplinary Optimization, 33(4): 375–386.
- [48] OHMORI, H. [2011]: *Computational Morphogenesis Its Current State and Possibility for the Future*. International Journal of Space Structures, 26(3): 269–276.

- [49] OLASON, A.; TIDMAN, D. [2010]: *Methodology for Topology and Shape Optimization in the Design Process*. Master thesis, Department of Applied Mechanics Division of Dynamics Chalmers University of Technology.
- [50] OSHER, S.J.; SANTOSA, F. [2001]: *Level Set Methods for Optimization Problems Involving Geometry and Constraints*. Journal of Computational Physics, 171(1): 272–288.
- [51] OTOMORI, M.; YAMADA, T.; IZUI, K.; NISHIWAKI, S. [2014]: *Matlab code for a level set-based topology optimization method using a reaction diffusion equation*. Structural and Multidisciplinary Optimization, 51(5): 1159–1172.
- [52] PROVATAS, N.; ELDER, K. [2011]: *Phase-Field Methods in Materials Science and Engineering*. John Wiley & Sons.
- [53] QIAN, X.; SIGMUND, O. [2013]: *Topological design of electromechanical actuators with robustness toward over- and under-etching*. Computer Methods in Applied Mechanics and Engineering, 253: 237–251.
- [54] RODRIGUES, H.; FERNANDES, P. [1995]: *A material based model for topology optimization of thermoelastic structures*. International Journal for Numerical Methods in Engineering, 38(12): 1951–1965.
- [55] ROJAS-LABANDA, S.; STOLPE, M. [2015]: *Automatic penalty continuation in structural topology optimization*. Structural and Multidisciplinary Optimization, 52(6): 1205–1221.
- [56] ROZVANY, G. I. N. [1998]: *Exact analytical solutions for some popular benchmark problems in topology optimization*. Structural optimization, 15(1): 42–48.
- [57] SCHRÖDER, J.; LABUSCH, M.; KEIP, M.-A. [2016]: *Algorithmic two-scale transition for magneto-electro-mechanically coupled problems FE2-scheme: Localization and homogenization*. Computer Methods in Applied Mechanics and Engineering, 302: 253–280.
- [58] SETHIAN, J.A.: *Evolution, Implementation, and Application of Level Set and Fast Marching Methods for Advancing Fronts*. Journal of Computational Physics, 169(2): 503–555.
- [59] SETHIAN, J.A. [1999]: *Level Set Methods and Fast Marching Methods: Evolving Interfaces in Computational Geometry, Fluid Mechanics, Computer Vision, and Materials Science ... and Computational Mathematics, Band 3*. Cambridge University Press, Cambridge, U.K. ; New York, 2 Edition.
- [60] SETHIAN, J.A.; WIEGMANN, A. [2000]: *Structural Boundary Design via Level Set and Immersed Interface Methods*. Journal of Computational Physics, 163(2): 489–528.
- [61] SHEN, J.; YANG, X. [2010]: *Numerical approximations of Allen-Cahn and Cahn-Hilliard equations*. Discrete and Continuous Dynamical Systems, 28(4): 1669–1691.
- [62] SIGMUND, O. [2001]: *A 99 Line Topology Optimization Code Written in Matlab*. Struct. Multidiscip. Optim., 21(2): 120–127.
- [63] SIGMUND, O. [2001]: *Design of multiphysics actuators using topology optimization - Part I: One-material structures*. Computer Methods in Applied Mechanics and Engineering, 190(49): 6577–6604.

- [64] SIGMUND, O. [2001]: *Design of multiphysics actuators using topology optimization - Part II: Two-material structures.* Computer Methods in Applied Mechanics and Engineering, 190(49): 6605–6627.
- [65] SIGMUND, O. [2007]: *Morphology-based black and white filters for topology optimization.* Structural and Multidisciplinary Optimization, 33(4-5): 401–424.
- [66] SIGMUND, O. [2009]: *Manufacturing tolerant topology optimization.* Acta Mechanica Sinica, 25(2): 227–239.
- [67] SIGMUND, O.; MAUTE, K. [2013]: *Topology optimization approaches.* Structural and Multidisciplinary Optimization, 48(6): 1031–1055.
- [68] SIGMUND, O.; PETERSSON, J. [1998]: *Numerical instabilities in topology optimization: A survey on procedures dealing with checkerboards, mesh-dependencies and local minima.* Structural optimization, 16(1): 68–75.
- [69] SIGMUND, O.; TORQUATO, S. [1999]: *Design of smart composite materials using topology optimization.* Smart Materials and Structures, 8(3): 365.
- [70] TAKEZAWA, A.; NISHIWAKI, S.; KITAMURA, M. [2010]: *Shape and topology optimization based on the phase field method and sensitivity analysis.* Journal of Computational Physics, 229(7): 2697–2718.
- [71] THURIER, P.F. [2014]: *A Two-material Topology Optimization Method for the Design of a Passive Thermal Control Interface.*
- [72] WALLIN, M.; IVARSSON, N.; RISTINMAA, M. [2015]: *Large strain phase-field-based multi-material topology optimization.* International Journal for Numerical Methods in Engineering, 104(9): 887–904.
- [73] WALLIN, M.; RISTINMAA, M. [2013]: *Howard's algorithm in a phase-field topology optimization approach.* International Journal for Numerical Methods in Engineering, 94(1): 43–59.
- [74] WALLIN, M.; RISTINMAA, M. [2014]: *Finite strain topology optimization based on phase-field regularization.* Structural and Multidisciplinary Optimization, 51(2): 305–317.
- [75] WANG, M.Y.; ZHOU, S. [2004]: *Phase field: A variational method for structural topology optimization.* Computer Modeling in Engineering & Sciences, 6(6): 547–566.
- [76] WHEELER, A. A.; BOETTINGER, W. J.; MCFADDEN, G. B. [1992]: *Phase-field model for isothermal phase transitions in binary alloys.* Physical Review A, 45(10): 7424–7439.
- [77] XIA, L.; BREITKOPF, P. [2014]: *A reduced multiscale model for nonlinear structural topology optimization.* Computer Methods in Applied Mechanics and Engineering, 280: 117–134.
- [78] XIA, L.; BREITKOPF, P. [2016]: *Recent Advances on Topology Optimization of Multiscale Nonlinear Structures.* Archives of Computational Methods in Engineering, pp. 1–23.
- [79] XIA, Q.; WANG, M. [2008]: *Topology optimization of thermoelastic structures using level set method.* Computational Mechanics, 42(6): 837.

- [80] YAMADA, T.; IZUI, K.; NISHIWAKI, S.; TAKEZAWA, A. [2010]: *A topology optimization method based on the level set method incorporating a fictitious interface energy.* Computer Methods in Applied Mechanics and Engineering, 199(45): 2876–2891.
- [81] ZHANG, W.H.; YANG, J.; XU, Y.; GAO, T. [2013]: *Topology optimization of thermoelastic structures: mean compliance minimization or elastic strain energy minimization.* Structural and Multidisciplinary Optimization, 49(3): 417–429.
- [82] ZUO, W.J.; SAITOU, K. [2016]: *Multi-material topology optimization using ordered SIMP interpolation.* Structural and Multidisciplinary Optimization, pp. 1–15.